Available online at www.sciencedirect.com
ScienceDirect
Geochimica et Cosmochimica Acta 74 (2010) 5884–5905
Geochimica et Cosmochimica Acta
www.elsevier.com/locate/gca

Ancient graphite in the Eoarchean quartz-pyroxene rocks from Akilia in southern West Greenland II: Isotopic and chemical compositions and comparison with Paleoproterozoic banded iron formations

Dominic Papineau [a,*], Bradley T. De Gregorio [b], Rhonda M. Stroud [b], Andrew Steele [a], Ernesto Pecoits [c], Kurt Konhauser [c], Jianhua Wang [d], Marilyn L. Fogel [a]

[a] Geophysical Laboratory, Carnegie Institution of Washington, Washington, DC 20015, USA
[b] Materials Science and Technology Division, Naval Research Laboratory, Washington, DC 20375-5320, USA
[c] Department of Earth Sciences, University of Alberta, Edmonton, Alberta, Canada
[d] Department of Terrestrial Magnetism, Carnegie Institution of Washington, Washington, DC 20015, USA

Received 19 February 2009; accepted in revised form 6 July 2010; available online 14 July 2010

Abstract

We present detailed petrographic surveys of apatite grains in association with carbonaceous material (CM) in two banded iron formations (BIFs) from the Paleoproterozoic of Uruguay and Michigan for comparison with similar mineral associations in the highly debated Akilia Quartz-pyroxene (Qp) rock. Petrographic and Raman spectroscopic surveys of these Paleoproterozoic BIFs show that apatite grains typically occur in bands parallel to bedding and are more often associated with CM when concentrations of organic matter are high. Carbonaceous material in the Vichadero BIF from Uruguay is generally well-crystallized graphite and occurs in concentrations around 0.01 wt% with an average $\delta^{13}C_{gra}$ value of $-28.6 \pm 4.4‰$ (1σ). In this BIF, only about 5% of apatite grains are associated with graphite. In comparison, CM in the Bijiki BIF from Michigan is also graphitic, but occurs in concentrations around 2.4 wt% with $\delta^{13}C_{gra}$ values around $-24.0 \pm 0.3‰$ (1σ). In the Bijiki BIF, more than 78% of apatite grains are associated with CM. Given the geologic context and high levels of CM in the Bijiki BIF, the significantly higher proportion of apatite grains associated with CM in this rock is interpreted to represent diagenetically altered biomass and shows that such diagenetic mineral associations can survive metamorphism up to the amphibolite facies.

Isotope compositions of CM in muffled acidified whole-rock powders from the Akilia Qp rock have average $\delta^{13}C_{gra}$ values of $-17.5 \pm 2.5‰$ (1σ), while $\delta^{13}C_{carb}$ values in whole-rock powders average $-4.0 \pm 1.0‰$ (1σ). Carbon isotope compositions of graphite associated with apatite and other minerals in the Akilia Qp rock were also measured with the NanoSIMS to have similar ranges of $\delta^{13}C_{gra}$ values averaging $-13.8 \pm 5.6‰$ (1σ). The NanoSIMS was also used to semi-quantitatively map the distributions of H, N, O, P, and S in graphite from the Akilia Qp rock, and relative abundances were found to be similar for graphite associated with apatite or with hornblende, calcite, and sulfides. These analyses revealed generally lower abundances of trace elements in the Akilia graphite compared to graphite associated with apatite from Paleoproterozoic BIFs.

Graphite associated with hornblende, calcite, and sulfides in the Akilia Qp rock was fluid-deposited at high-temperature from carbon-bearing fluids, and since this graphite has similar ranges of $\delta^{13}C_{gra}$ values and of trace elements compared to graphite associated with apatite, we conclude that the Akilia graphite in different mineral associations formed from the same source(s) of CM. Collectively our results do not exclude a biogenic origin of the carbon in the Akilia graphite, but because some observations can not exclude graphitization of abiogenic carbon from CO_2- and CH_4-bearing mantle fluids, there remain ambiguities with respect to the exact origin of carbon in this ancient metasedimentary rock. Accordingly, there

* Corresponding author. Tel.: +1 202 478 8908; mobile: +1 303 514 8978; fax: +1 202 478 8901.
E-mail address: dpapineau@ciw.edu (D. Papineau).

doi:10.1016/j.gca.2010.07.002

may have been several generations of graphite formation along with possibly varying mixtures of CO_2- and CH_4-bearing fluids that may have resulted in large ranges of $\delta^{13}C_{gra}$ values. The possibility of fluid-deposited graphite associated with apatite should be a focus of future investigations as this may prove to be an alternative pathway of graphitization from phosphate-bearing fluids. Correlated micro-analytical approaches tested on terrestrial rocks in this work provide insights into the origin of carbon in ancient graphite and will pave the way for the search for life on other ancient planetary surfaces.

1. INTRODUCTION

Since the report of ^{13}C-depleted graphite associated with apatite in the >3.83 Ga Qp rock from the island of Akilia in southern West Greenland (Mojzsis et al., 1996), this rock has become symbolic of the challenges facing the recognition of the remains of early life on Earth. These mineral associations were originally interpreted as evidence of the emergence of life earlier than 3.83 Ga. This interpretation has prompted an intense effort to study the Akilia Quartz-pyroxene (Qp) rock, and resulted in conflicting interpretations on its protolith, age, and the existence of graphite associated with apatite. Major and minor minerals of the Eoarchean Akilia Qp rock include quartz, hedenbergite, ferrosilite, hornblende–grunerite, magnetite, pyrrhotite, chalcopyrite, and garnet, while accessory phases include pentlandite, zircon, apatite, and calcite (Papineau et al., 2010). Graphite is also present. The occurrence of pyroxenes and amphiboles in this highly metamorphosed ferruginous sedimentary rock is expected from high-temperature reactions either between Fe-carbonate and quartz, or between Fe-silicates or magnetite and quartz with metasomatic fluids (James, 1955; French, 1964, 1968, 1973; Klein, 1973, 1978, 2005; Schreyer et al., 1978).

The original interpretation that the protolith of the Akilia Qp rock is an iron formation that precipitated from seawater (McGregor and Mason, 1977; Mojzsis et al., 1996, 2003; Nutman et al., 1997; Friend et al., 2002; Mojzsis and Harrison, 2002a,b; Dauphas et al., 2004, 2007; Manning et al., 2006; Nutman and Friend, 2006; McKeegan et al., 2007) has been countered by other groups who have proposed that this rock formed from the metasomatic replacement of an ultramafic protolith (Fedo and Whitehouse, 2002a,b, 2007; Whitehouse and Fedo, 2003; Bolhar et al., 2004; André et al., 2006; Fedo et al., 2006; Whitehouse et al., 2009). Age constraints on the Qp rock were initially determined to be >3.85 Ga (Nutman et al., 1997), but this has also been debated (Sano et al., 1999; Myers and Crowley, 2000; Whitehouse and Kamber, 2005). Depth profile analyses of single zircons from orthogneisses on Akilia have revealed evidence for several phases of zircon growth at 3.83, 3.73, 3.65 and 2.66 Ga (Mojzsis and Harrison, 2002; Manning et al., 2006). However, similar U–Pb age data from zircons in other orthogneisses on Akilia were alternatively interpreted to indicate that 3.83 Ga zircons were inherited in a 3.62 Ga original tonalitic melt that was subsequently metamorphosed around 2.7 Ga and again around 1.7 Ga (Whitehouse and Kamber, 2005; Whitehouse et al., 2009). Additional U–Pb analyses on apatites have been used to argue that the age of these minerals in the Akilia Qp rock is around 1.7 Ga (Sano et al., 1999; Whitehouse et al., 2009), but this may also be due to metamorphic re-equilibration around 1.7 Ga. While the protolith and age constraints of the Akilia Qp rock are still being debated, much work remains to be done to elucidate the pathways of carbon that led to graphite formation in this rock.

Isotopically light carbon in graphite frequently associated with apatite from the Akilia Qp rock (Mojzsis et al., 1996; McKeegan et al., 2007) has also been a source of debate. Recent petrographic analyses of thin sections of the Qp rock have failed to verify that apatite–graphite associations are common, including from the original sample G91-26 (Lepland et al., 2005; Nutman and Friend, 2006). This may have been partly due to the method of grain separation used by some of these groups to find graphite associated with apatite. Recently, detailed surveys of thin sections from sample G91-26 by transmitted light microscopy at 200–400× magnification along with confocal Raman microspectroscopic imaging have demonstrated that these mineral associations are indeed frequent in the Akilia Qp rock (Papineau et al., 2010). However, the presence of graphite inclusions sensu stricto within apatite grains has not yet been confirmed directly by scanning electron microscopy (SEM), focused ion beam (FIB), or transmission electron microscopy (TEM) (Papineau et al., 2010).

Because the carbon isotope composition of ancient carbonaceous material (CM) alone is not a robust indicator of biogenecity in metasedimentary rocks (Horita, 2005), possible abiogenic sources of carbon in graphite need to be thoroughly investigated. Carbonaceous material associated with magnetite and carbonate from terrestrial and martian mantle rocks has been attributed to the decarbonation of siderite or other abiogenic precursor phases formed from CO_2-rich mantle fluids (Steele et al., 2007). Metamorphic fluids can produce or transport organic compounds synthesized via abiotic synthesis reactions such as Fischer–Tropsch type (FTT) reactions through the catalyzed reduction of CO_2, HCO_3, or CO by H_2 from fluid–rock interactions (McCollom and Seewald, 2006). In addition, there is always the possibility of later contamination and infiltration, but this can usually be eliminated by Raman spectra of CM that are consistent with the metamorphic grade of the host rock. Therefore, graphite in the oldest metasedimentary rocks in the geological record must be carefully evaluated in order to constrain the possible origins of its carbon.

A related problem is to determine the origin of CM associated with phosphatic minerals in highly metamorphosed sedimentary rocks. Multiple criteria are necessary to ascertain the pathways of carbon in graphite and correlated micro-analytical techniques can provide valuable constraints. The residual presence of heteroatoms such as N,

S, and P in CM from metasedimentary rocks may potentially be indicative of a biological origin if abiogenic sources of carbon can be excluded (De Gregorio et al., 2009). The presence of phosphate minerals intimately associated with CM may be another biosignature, although this also remains to be demonstrated. These mineral associations may form from the diagenetic maturation of CM because phosphate is released from CM into interstitial pore water during diagenesis, and can then react with calcium to precipitate as carbonate–fluorapatite (Van Cappellen and Berner, 1988). Indeed, rocks rich in phosphate, such as phosphorites, often contain relatively high amounts of biogenic CM commonly associated with carbonate–fluorapatite (Papineau, 2010 and references therein).

To address this problem for CM associated with apatite in the Eoarchean Akilia Qp rock, we used multiple micro-analytical techniques to characterize in situ its chemical and isotopic compositions. Geochemical datasets for graphite in its petrographic context within the Akilia Qp rock are then directly compared to similar apatite associations with CM from two Paleoproterozoic BIFs from Uruguay and Michigan metamorphosed at the upper amphibolite and amphibolite facies, respectively. Such comparisons with younger sedimentary strata are necessary to establish a broader geologic context for CM associated with apatite.

2. SAMPLE DESCRIPTIONS

Two samples of BIFs were selected for comparison with the Akilia Qp rock. These were selected on the basis of similarities in metamorphic grades with the Akilia Qp rock, the presence of apatite grains associated with graphite, and depositional ages at a time when life was flourishing. Their different mineralogy illustrates that graphite associations with apatite occur in a wide variety of iron formations.

2.1. Vichadero BIF – 050809/2 (Vichadero Formation, Departamento de Rivera, Uruguay)

BIFs occur at several localities in the northeast of Uruguay. One notable occurrence is in the Zapucay Mineral District and has characteristics similar to co-eval BIFs in the nearby Quadrilatero Ferrífero in Brazil. The region contains an extensive and relatively well-exposed Paleoproterozoic supracrustal sequence (Vichadero Formation), which strikes approximately NW–SE along the surrounding Archean basement. These rocks were intensively deformed and metamorphosed during a Paleoproterozoic tectonothermal event between 2.1 and 1.7 Ga. This peak of regional metamorphism overprinted the sequence under upper amphibolite to granulite facies conditions and is considered to be of Transamazonian age as suggested by Rb–Sr isochrons of about 2.27 Ga (Cordani and Solani, 1990). The Vichadero Formation is approximately 100 m thick and is composed of BIFs, manganese-formations, quartzites, calc-silicate rocks, and basic metavolcanics (Ellis, 1998). The BIFs are dominated by meso- and micro-bands with alternating silica and iron-rich layers, which predominantly consist of quartz, Fe–Mn–oxides, amphibole, clinopyroxene, garnet, olivine, and braunite.

2.2. TVA294-659.6 – Bijiki member of the Michigamme Formation, Michigan, United States

A hand sample from the Bijiki iron formation was collected from drill core TVA 29-4 in Marquette, Michigan at a depth of 201.0 m (or 659.6 feet down-core – sample TVA294-659.6 hereafter). The Bijiki member of the Paleoproterozoic Michigamme Formation is stratigraphically near the top of the Baraga Group of the Marquette Supergroup. The Baraga Group was deposited during the Penokean orogeny between 1.874 and 1.833 Ga (Schneider et al., 2002; Schulz and Cannon, 2007) and has been dated at approximately 1.852 Ga (Sims et al., 1989). Sediments of the Baraga Group were buried quickly and were highly metamorphosed shortly after deposition during the northward advancing trust of the Penokean orogeny (Schulz and Cannon, 2007). This section of the drill core is a magnetic shaley and sulfidic BIF with high concentrations of organic matter and also contains carbonate. Small garnet and grunerite grains are occasionally present in other parts of this drill core, which suggest an overall metamorphic grade around the amphibolite facies. Exposure to an ammonium molybdate and HNO_3 solution yielded a yellow color upon contact with the rock, indicating an abundance of phosphate minerals. Petrographic observations of the mineral assemblage revealed the presence of ferruginous silicates (e.g. grunerite), magnetite, dolomite (with minor Fe), chalcopyrite, pyrite, apatite, and graphitic CM.

3. ANALYTICAL METHODS

3.1. Optical microscopy

Optical microscopy was used to perform apatite surveys in one ~2.7 × 4.6 cm polished thin section (~30 μm thick) of BIF sample 050809/2 from the Vichadero Formation. An Olympus Bx61 microscope with 10×, 40×, and 100× long working-distance objectives was used without immersion oil to map apatite grains. Apatite occurrences in one 1-cm diameter polished slab of sample TVA294-6596 from the Bijiki BIF were mapped by back-scattered electron (BSE) microscopy (see below). Apatite maps of thin sections from sample G91-26 from the Akilia Qp rock revealed that ~18% of apatite grains had graphite coatings, which is reported in Papineau et al. (2010).

3.2. Raman spectroscopy

Raman spectroscopy was used to characterize the structural ordering of CM in the Paleoproterozoic BIFs. The maturity of CM can be directly correlated to metamorphic grades and can be evaluated from the characteristic D- and G-bands (around 1340 cm^{-1} and 1590 cm^{-1}, respectively – Beyssac et al., 2002; Wopenka and Pasteris, 1993). Detailed descriptions of Raman methods are presented in Papineau et al. (2010). In brief, confocal laser Raman spectroscopy was performed with WITec a-SNOM imaging system using a 532 nm laser under 1000× magnification. A 100 or 50 μm diameter optic fiber was used to collect data in imaging mode. A Raman spectrum was acquired for each pixel with

a dwell time between 0.6 and 2 s, producing hyperspectral datasets with a spatial resolution around 360 nm using the 100× objective (0.9 N.A. – Steele et al., 2007). Hyperspectral images of specific mineral phases were generated by mapping peak intensity from spectral datasets and include information on chemical composition and latent crystal strain (Bernard et al., 2008). Polishing during sample preparation can disrupt the crystal structure of graphite and cause flaking, leading to a more intense and broadened D-band than the original unaltered graphite (Pasteris, 1989; Papineau et al., 2010). This was avoided by collecting spectra at least 1 μm and deeper below the thin section surface.

3.3. Scanning electron microscopy

Detailed methods for imaging samples using scanning electron microscopy (SEM) are described in Papineau et al. (2010). In brief, these observations were performed with a JEOL 6500F field-emission SEM using a 15 kV accelerating voltage potential and electron beam current of either 0.5 or 1 nA. Images were acquired using both secondary (SE) and back-scattered (BSE) electrons. To minimize surface contamination by carbon-containing compounds during the final two steps of the polishing process, samples were manipulated with nitrile gloves and polished with 99.9% pure Cerium oxide powder (3 and 0.5 μm) and DI water on a muffled glass plate. Samples were subsequently washed at least five times in DI water and ultrasound baths, followed by drying at 80 °C, and gently blowing Ar gas on the surface. Samples were then stored in muffled vials with muffled Al foil caps in a vacuum oven. One-centimeter diameter slabs were prepared for analysis with the NanoSIMS by ion-milling using a ~1 mA Ar^+ beam at 70° from normal incidence under an accelerating voltage of 8 keV. Ar-milling for 60 min under constant rotation in relatively low vacuum (0.175 torr) greatly decreased surface topography of graphite (Electronic Annex 1). Samples were subsequently coated with gold and targets of interest were located by BSE and SE imaging. Exposure time to the electron beam in the SEM was kept low to minimize the deposition of carbon films on the gold coat in the vicinity of the targets.

3.4. Isotope ratio mass spectrometry

Polished slabs of sample G91-26 were manipulated with nitrile gloves and washed several times in DI water followed by an ultrasonication cleaning step in dichloromethane to minimize surface contamination. The carbon isotope composition of CM in the Akilia Qp rock was measured on bulk powders. For bulk powders, Akilia sample G91-26 was subdivided into four blocks representing the coarse-grained quartz-rich area (sub-sample AB) and the fine-grained pyroxene-rich areas (CD, E, and F). Bulk powders were generated with a ceramic shatter box rinsed several times with DI water and cleaned at least twice with pure quartz chips muffled at 550 °C for 4 h. Total organic carbon analyses were performed with a CE Instruments NA 2500 series elemental analyzer (EA) linked to a Thermofisher Delta V Plus IRMS through a Conflo III interface. Samples were combusted at 1020 °C in the presence of ultrapure O_2 in a continuous flow of He carrier gas. Isotopic standard CO_2 gas was alternatively injected with the sample gases for calibration. These analyses were challenging because of the low carbon concentrations, especially in the Akilia Qp rock, and because of microscopic heterogeneities in powdered samples.

Typically around 5 mg of powdered sample, but up to 30 mg for carbon-poor samples, was weighed in Ag boats pre-muffled at 550 °C for 2 h. Analyses of untreated powders were first performed to determine the total amount of carbon in the powdered samples. This was followed by analyses of aliquots from the same powders muffled at 550 °C for 2–4 h, in an effort to remove possible organic contaminants from the modern environment or sample preparation. Aliquots of muffled powders were subsequently decarbonated with ultra pure 6 N HCl (Sequanal Grade, Pierce) to determine the isotope composition of graphite in bulk powders. Analyses of 1–6 μg of organic carbon from a compositionally similar standard (Peru mud; $\delta^{13}C_{org} = -20.2‰$, TOC = 6.6 wt%) gave a 1σ reproducibility better than ±0.8‰ for $\delta^{13}C$ and ±5% for total organic carbon (TOC – although it is around ±45% for samples with low C (e.g. <0.1 wt%)). Combustion experiments on graphite (USGS 24 and CH graphites) mixed with pure quartz were performed to test for possible matrix effects during muffling at 550 °C. Results showed that muffling about 1 wt% of graphite mixed with quartz causes insignificant change in $\delta^{13}C$ values and that the carbon concentration remains unaffected, within analytical error. The muffled Ag boat contained less than 0.06 μg of carbon, and typically less than the detection limit of around 0.04 μg.

Carbonate carbon isotopes were measured on about 40 mg of whole-rock powders from the four different splits of the G91-26 slab with a Gas Bench, also in continuous flow. Bulk rock powders inserted in exetainer vials were reacted with 99.9% pure phosphoric acid at 70 °C. Ultrapure He carrier gas then flowed through the exetainers and the evolved gas was dehydrated and chromatographically purified prior to its introduction in the IRMS. Analyses of carbonate standards NBS 18, NBS 19, and two in-house calcite and dolomite standards gave a reproducibility of better than 0.2‰ for $\delta^{13}C_{carb}$ and 0.3‰ for $\delta^{18}O_{carb}$. All carbonate isotope analyses are reported with respect to the PDB standard.

3.5. Analyses with the NanoSIMS

NanoSIMS-based carbon isotope analyses and elemental maps were obtained with the third-generation ion microprobe NanoSIMS 50L at the Carnegie Institution of Washington. Carbon isotope analyses were performed using a Cs^+ primary beam of about 200 pA with an accelerating voltage of 8 kV, while a smaller 1.5 pA beam was used for elemental mapping. These analyses were performed under ultra-high vacuum around 2×10^{-9} torr. For carbon isotopes, the instrument was tuned for a mass resolving power around 8000, while a higher mass resolving power of 9000 was needed for elemental mapping in order to resolve $^{12}C^1H^-$ from $^{13}C^-$ and $^{12}C^{14}N^-$ from $^{13}C_2^-$. A

normal incidence electron gun was used for charge compensation and a nuclear magnetic resonance magnetic field stabilizer was used for all analyses.

For carbon isotope analyses, the primary beam was rastered over a 4×4 μm region on each target. Each analysis consisted of 10 cycles of pre-sputtering with a slightly defocused primary beam (~60 s) followed by 100 blocks of 10 cycles each. Faraday cup collectors were used for both ^{12}C and ^{13}C. Instrumental mass fractionation (IMF) was corrected using analyses of pure graphite from Sri Lanka ($\delta^{13}C = -8.2‰$). Analyses on diamond standard 4139 ($\delta^{13}C = -4.0‰$) were also used for comparison. A small linear drift in $^{12}C/^{13}C$ during the analytical session was corrected in the data. To observe the effective removal of graphitic material by the Cs^+ beam, analyzed targets were subsequently imaged by SE (Electronic Annex 2). Variations in surface topography of graphite are known to affect IMF to a minor extent (<1‰) in conventional SIMS analyses using primary ion beam spot sizes between 20 and 50 μm (Farquhar et al., 1999). Minor IMF effects of less than 0.5‰ may also arise from variable crystallographic orientations of graphite flakes (Farquhar et al., 1999). Similar carbon isotope analyses on 4×4 μm spots by SIMS using a primary beam current of 1–2 pA and electron-multiplier detectors give a 2σ reproducibility of about 2‰ (Fletcher et al., 2008). Graphite targets only from Akilia sample G91-26 were analyzed in this work.

Elemental maps were generated with the NanoSIMS by detecting the secondary ions ^{12}C, $^{12}C^1H$, $^{12}C^{14}N$, ^{16}O, ^{31}P, and ^{32}S simultaneously on electron-multiplier detectors. Secondary ion counts relative to ^{12}C represent first-order semi-quantitative estimates for comparisons of elemental abundance between different targets. These estimates are only semi-quantitative however, because a suitable suite of graphite standards with homogeneous H, O, N, P, and S abundances, necessary to normalize actual atomic abundances of these elements, was unavailable. Estimates of relative secondary ion counts therefore do not reflect actual atomic ratios because the sputtered secondary ions have different ionization efficiencies. However, in an attempt to quantitatively constrain levels of N in graphite targets analyzed by NanoSIMS, we independently measured N abundances by EA-IRMS in the graphites from Mt. Kearsarge (600 ± 48 ppm; $n = 3$) and Sri Lanka (176 ± 51 ppm; $n = 2$), which was in the range expected for poorly crystalline graphite (Ader et al., 2006). This was performed by mixing 1–3 mg of graphite powder with up to 2–3 times more V_2O_5 to help the combustion and to minimize the contribution of isobaric interference by CO from impartial combustion. These graphites, however, may not necessarily have homogeneous N concentrations.

Each NanoSIMS elemental map analysis consisted of 10 cycles of pre-sputtering with a defocused primary beam (~10 min at 1.5 nA) on a slightly larger area than the imaged target followed by 50–60 measurement cycles (80–90 min total) to ensure beam stability and achieve stable count rates. Typically only the last 20 cycles or so, after the count rates were stable and had reached a plateau, were used for data analysis. Imaged regions were generally around 10×10 μm. Secondary ion images were processed with the L'image software package (L.R. Nittler, Carnegie Institution of Washington) to generate a series of elemental maps. Uniformity in secondary ion maps is highly sensitive to the topography of targets and artifacts can appear as gradients of secondary ion counts if the target deviates from a perfectly flat surface and as very bright or dark areas along cracks and holes.

These types of analyses with the NanoSIMS are also susceptible to various sources of nanometer-scale contaminants on typical polished sample surfaces. However, additional cleaning steps were performed (Section 3.3) to minimize surface contamination. During the 10 min long pre-sputtering steps before each acquisition, any residual surface contamination should have been eliminated, although implantation of residual surface contaminants within the target cannot be entirely excluded. After steady secondary ion counts were achieved, typical variations in secondary ion ratios were less than 10%. A typical set of 20 cycles of secondary ion ratios illustrates minor variations in secondary ion counts and relatively small ranges of ratios (Electronic Annex 3). For sample G91-26, graphite targets analyzed were associated with various minerals, including apatite, whereas for samples 50809/2 and TVA294-659.6 only CM associated with apatite was analyzed. Two fluid-deposited graphites from Mt. Kearsarge (New Hampshire) and Sri Lanka were analyzed in the same way for comparison. These graphites are thought to have precipitated from CO_2–CH_4 rich fluids that sourced carbon from the sedimentary host protolith or from nearby metasedimentary rocks (Rumble and Hoering, 1986; Rumble et al., 1986; Farquhar and Chacko, 1991; Farquhar et al., 1999).

4. RESULTS

4.1. Carbonaceous material associated with apatite in the petrographic context

Graphite associations with apatite in the Akilia Qp rock have been mapped in their petrographic context and analyzed by Raman microspectroscopy (Papineau et al., 2010). All graphite associations with apatite observed in G91-26 with BSE imaging occurred as thin coatings at the interface between apatite and quartz (see examples in Fig. 1). Apatite grains in thin sections of the fine-grained parts of the Akilia Qp rock ranged in size between 3 and 80 μm and about 18% of them were associated with graphite (Papineau et al., 2010).

Apatite grains in Vichadero BIF sample 50809/2 from Uruguay tended to be large (up to 250 μm) and rounded subhedral crystals occurring within quartz between bands of hematite and magnetite (Fig. 2). A total of 1827 apatite grains were identified and located in this thin section and graphite was found in association with 87 of these apatite grains (about 5% of apatites; Fig. 3a and b), less common than in the Akilia Qp rock. Large apatite grains often occurred in association with fine hematite rims (Fig. 3c and d), especially when they were located near Fe-rich bands. Fine-grained hematite also occasionally formed coatings on these apatite grains and this metamorphic remobilization of ferric iron occurred before the partial (Fig. 3e and f), and

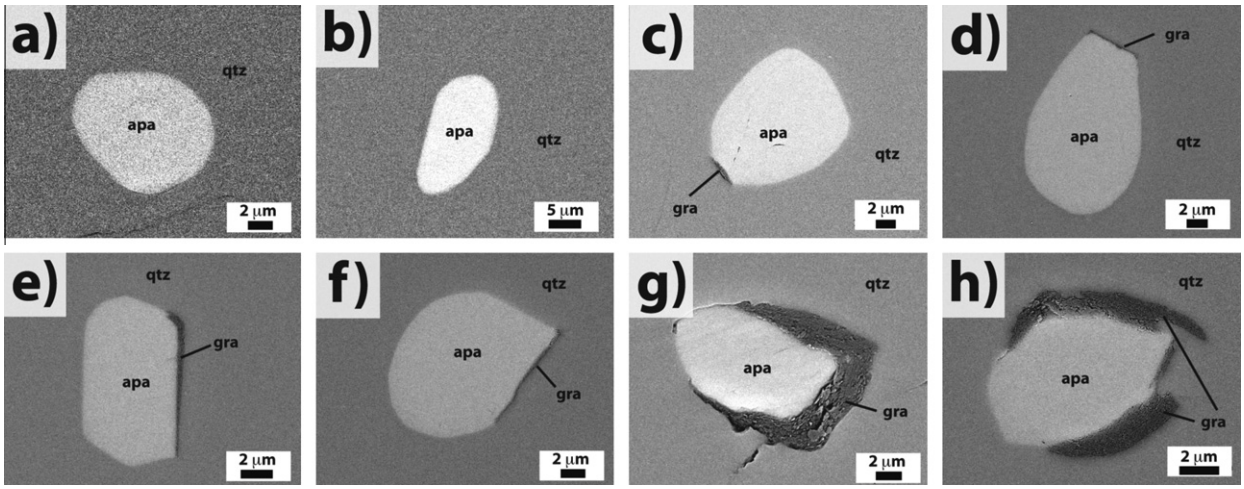

Fig. 1. Representative BSE images of apatite grains in Akilia Qp rock sample G91-26 showing individual apatite grains in the quartz matrix in (a) and (b), graphite coatings onto apatite grains in (c), (d), (e), and (f), and graphitic envelopes coating apatite grains in (g) and (h).

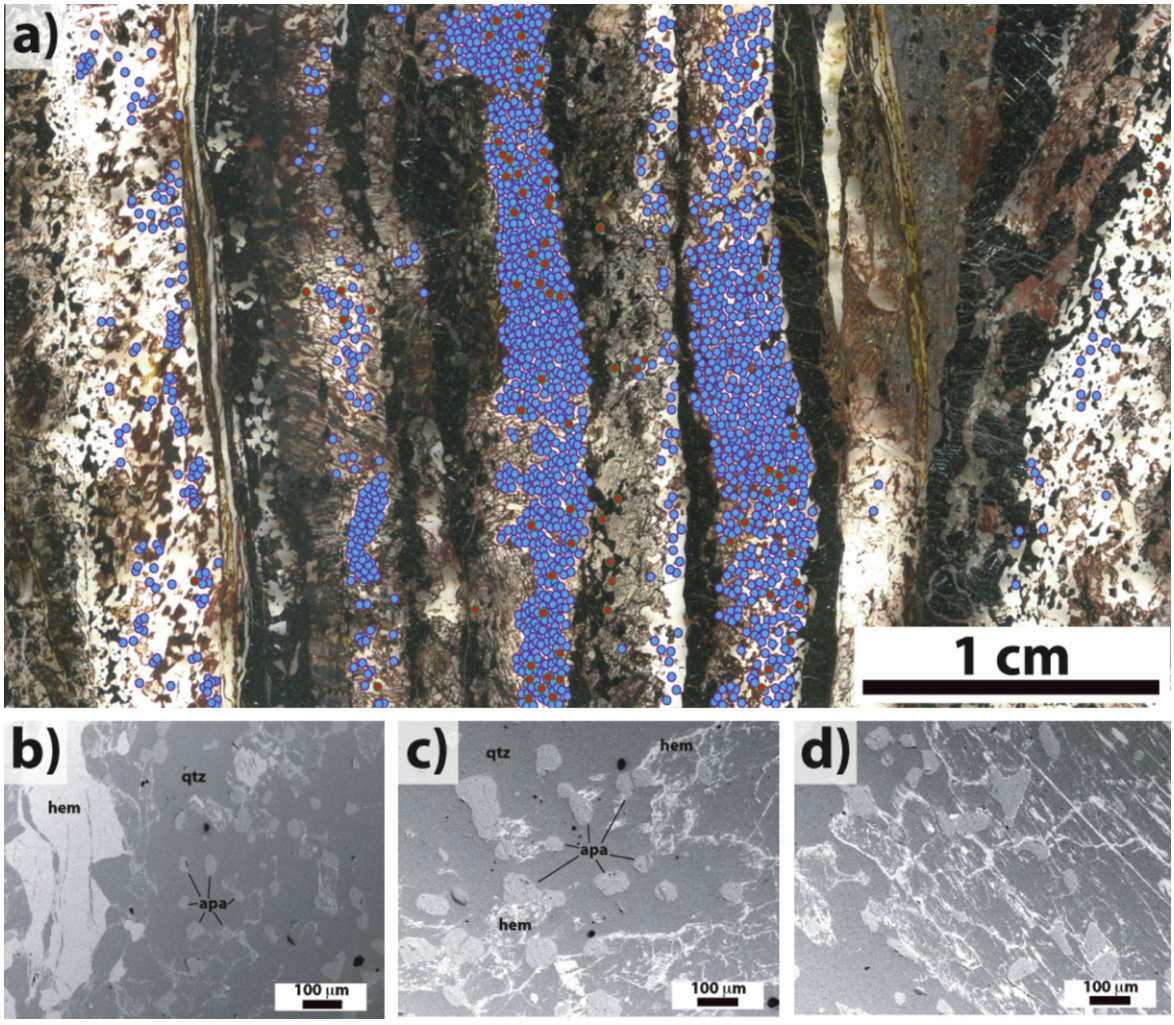

Fig. 2. (a) Thin section of the Vichadero BIF with 1827 mapped apatite grains distributed as bands showing apatites associated with graphite in red and those without in blue; (b–d) back-scattered electron images of representative fields of apatite grains in quartz, sometimes mixed with fine smears and rounded structures of microcrystalline hematite. Mineral abbreviations are: apa, apatite; hem, hematite; qtz, quartz.

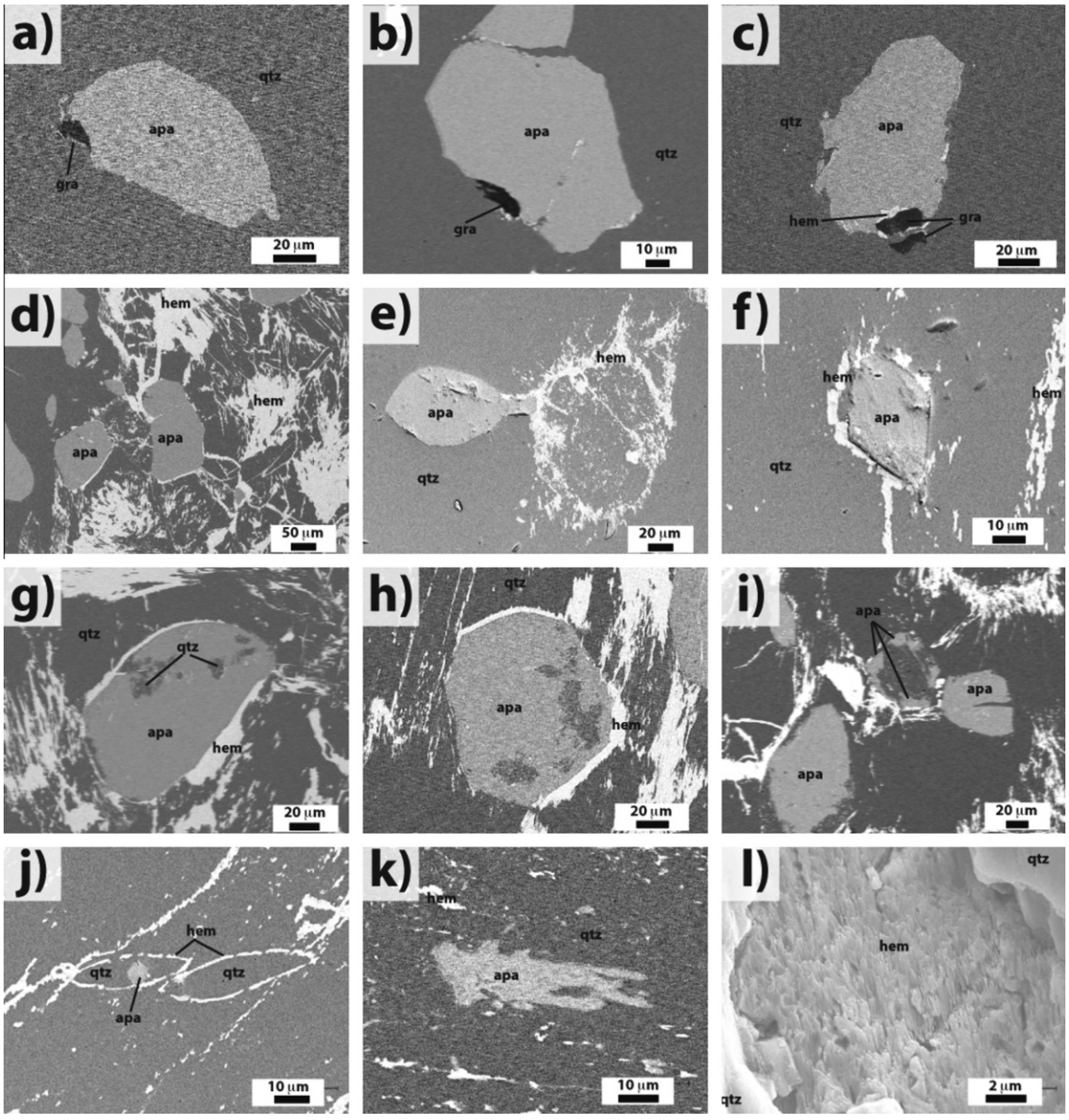

Fig. 3. Back-scattered electron images of apatite grains associated with hematite and quartz from the Vichadero BIF. Images (a) and (b) show examples of apatite-associated graphite, while (c) and (d) show different textures of hematite associated with apatite, and images (e)–(h) show the progressive replacement of apatite with quartz often rimed with microcrystalline hematite. In (i)–(k) are relatively rare anhedral apatite occurrences. Mineral abbreviations are: apa, apatite; gra, graphite; hem, hematite; qtz, quartz.

sometimes total (Fig. 3g and h), replacement of apatite by quartz. Partial replacement textures were not observed on apatite grains associated with graphite (Fig. 3a and b), as they were associated with relatively little hematite, which possibly relates to a more pristine and less disturbed mineral association. Small and rare anhedral apatite grains were also observed in finely disseminated hematite areas (Fig. 3i) and may represent metasomatically remobilized apatite. Ferric oxyhydroxides remobilized during metamorphism typically became finely disseminated hematite in the quartz matrix and had microcrystalline textures that formed small amorphous patches and veinlets.

A detailed petrographic survey of apatite grains in a $\sim$0.7 cm^2 slab from Bijiki BIF sample TVA294-659.6 from Michigan by BSE microscopy revealed a total of 658 apatite grains, of which more than 514 grains (or 78%) were associated with CM (Fig. 4a). In the Bijiki BIF, apatite grain sizes varied between 2 and $\sim$60 μm and they were generally associated with CM in the form of coatings and inclusions, sensu stricto. Apatite grains occurred almost exclusively in dolomite and tended to form bands parallel to bedding. They rarely occurred within magnetite (Fig. 4i). Dolomite bands were found parallel to bedding planes, but also as veins that cross-cut layers of the Fe-silicate matrix

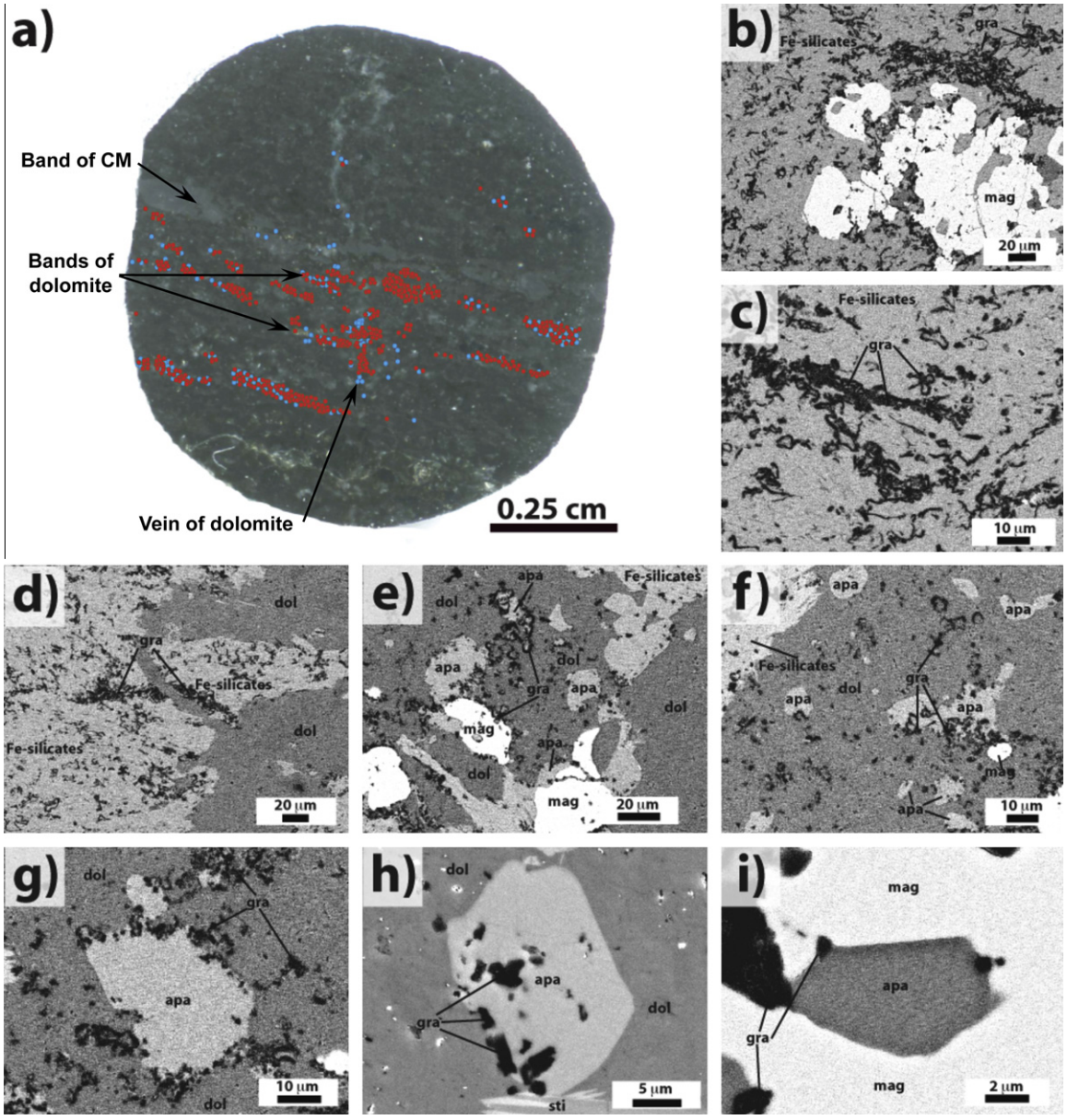

Fig. 4. (a) Polished slab of Bijiki BIF sample showing 658 mapped apatite grains distributed as bands and showing apatites associated with CM in red and those without in blue. Petrographic observations by BSE show (b and c) convoluted filaments of CM in Fe-silicate matrix and sometimes associated with magnetite, (d) a late diagenetic or metamorphically remobilized dolomite vein in the Fe-silicate matrix, (e and f) fields of apatite grains associated with CM in the dolomite matrix, (g and h) examples of individual apatite grains associated with CM in dolomite matrix, and (i) a rare apatite grain inside late diagenetic or metamorphic anhedral magnetite.

(Fig. 4d). In dolomite, CM occurred as fine amorphous disseminations with occasional rounded filamentous structures (Fig. 4e and f). Notably, these diagenetic dolomite veins and bands contained subhedral apatite grains associated with CM (Fig. 4e–h). In the Fe-silicate matrix, filamentous carbonaceous material also typically displayed convoluted, rounded, or curved structures (Fig. 4b–d).

4.2. Raman spectroscopy of CM associated apatite

A selection of apatite grains associated with CM in the Vichadero BIF sample 50809/2 was analyzed by Raman spectroscopy (Fig. 5d–i). Small hematite aggregates were also associated with CM in some of these targets (Fig. 5d, e, g, and i). Small calcite crystals were occasionally observed as inclusions in apatite (Fig. 5d, arrows) or in direct contact with CM, apatite, and quartz (Fig. 5f and h). Average Raman spectra extracted from these hyperspectral images revealed crystalline graphite that exhibited a strong G-band around 1575 cm^{-1} and a generally weak D-band around 1347 cm^{-1} (Fig. 6). In one graphite target (Fig. 5i), a 1 µm spot of graphite showed an unusually strong 2D-band around 2700 cm^{-1} (Fig. 6) similar to a few curled graphite structures discovered in the Akilia Qp rock (Papineau et al., 2010). Overall, the Ra-

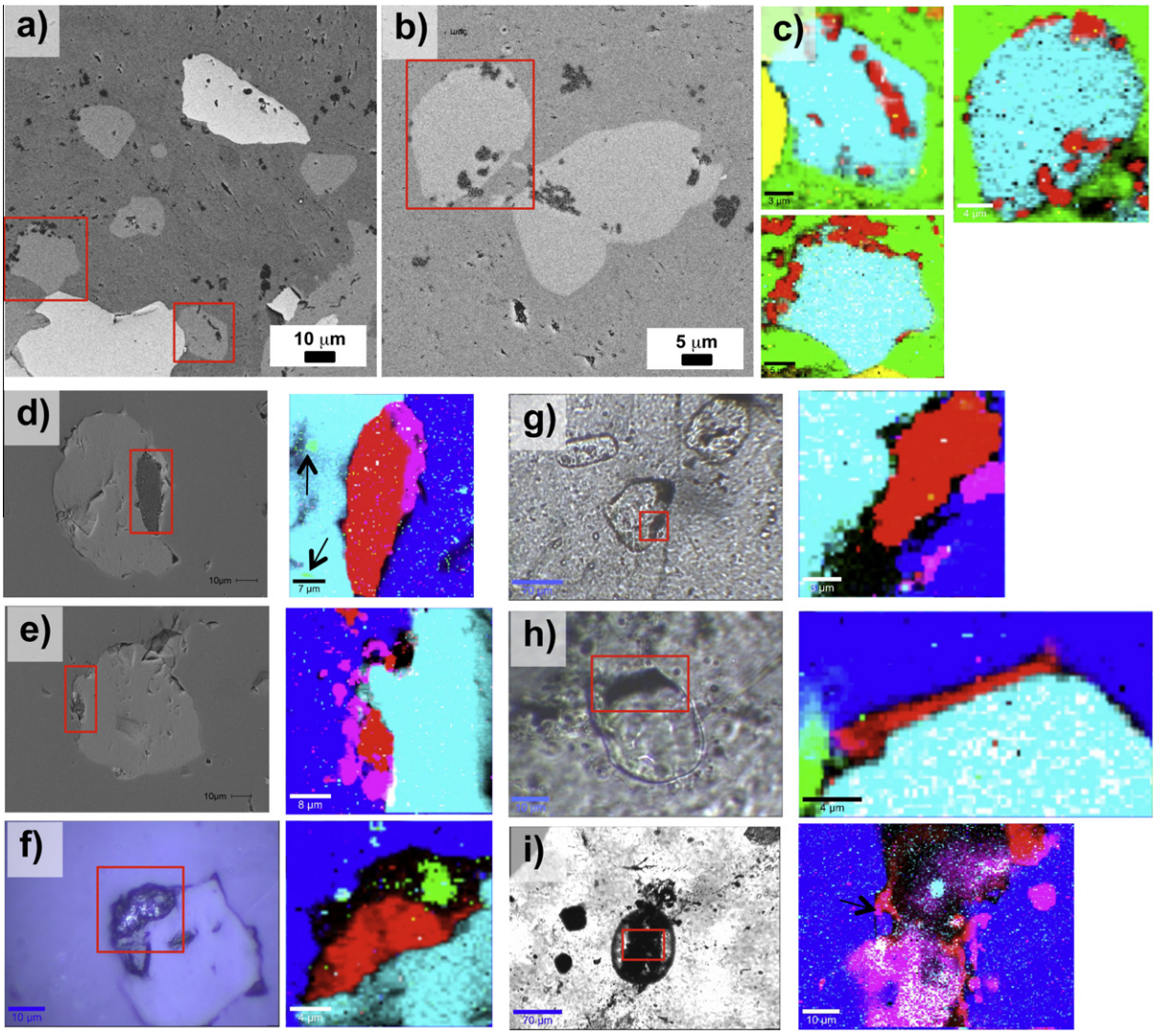

Fig. 5. Raman hyperspectral images of carbonaceous material associated with apatite in the BIF from (a–c) the Bijiki member of the Michigamme Formation and (d–i) the Vichadero Formation. The locations of Raman hyperspectral scans are indicated with red boxes in their petrographic context shown in back-scattered electron (a, b, d, and e), reflected light (f) and transmitted light (g–i). Mineral phases are carbonate (green), apatite (turquoise), carbonaceous material (red), magnetite (yellow), and hematite (purple). Black areas represent holes in the thin section.

man spectral characteristics and crystallinity of graphitic CM in the Vichadero BIF were similar to those of graphite in the Akilia Qp rock (Table 1 and Electronic Annex 4), and point to crystallization of indigenous CM during peak metamorphic conditions during the Transamazonian tectonothermal event around 2.27 Ga. Raman spectra of apatite crystals associated with these graphite particles (Electronic Annexes 5 and 6) exhibited the characteristic P–O peak at 965 cm^{-1} along with a series of characteristic peaks between 2000 and 2700 cm^{-1}.

Carbonaceous material associated with apatite in the Bijiki BIF from Michigan also displayed Raman spectroscopic characteristics of crystalline graphite (Figs. 5a–c and 6). Notably, the D-band FWHM, the positions of the G-band and 2D-band, and the D/G intensity ratio, have similar ranges as for CM from the Vichadero BIFs and from the Akilia Qp rock (Table 1 and Electronic Annex 4). These ranges imply a high degree of crystallinity of CM in the Bijiki BIF and indicate crystallization during peak metamorphic conditions, which occurred between 1.874 and 1.833 Ga during the Penokean orogeny (Schulz and Cannon, 2007).

4.2.1. Isotope composition of graphite in bulk powders

Carbon isotope analyses of untreated whole-rock powders from four Akilia sub-samples of G91-26 yielded an average $\delta^{13}C$ composition of $-10.2 \pm 4.9‰$ (1σ) for total carbon ($\delta^{13}C$ values ranged between -4.7 and $-17.8‰$; Table 2), which was in concentration averaging 0.078 ± 0.048 wt% (1σ). Aliquots of powders muffled at 550 °C yielded a similar average $\delta^{13}C$ composition of $-9.6 \pm 4.0‰$ (1σ) for total carbon ($\delta^{13}C$ values between $-4.6‰$

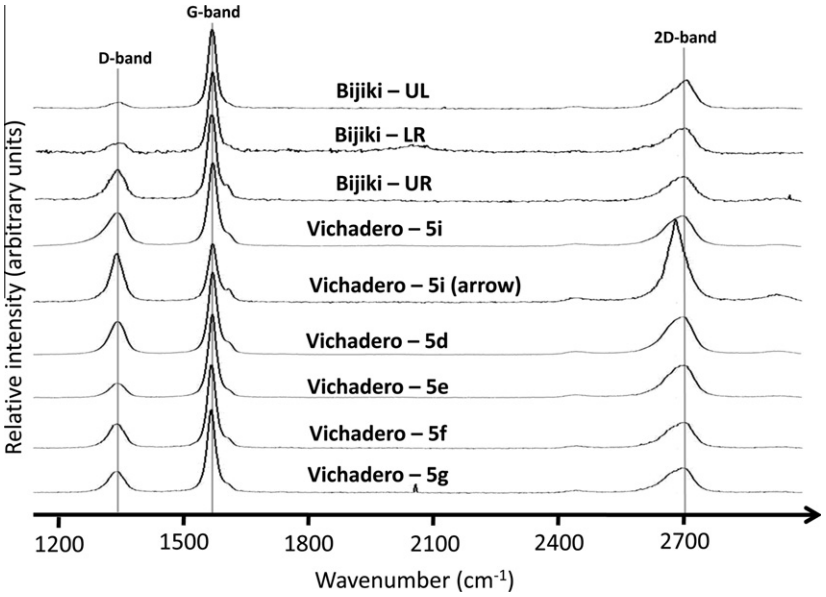

Fig. 6. Average Raman spectra of CM for the corresponding targets in Fig. 5.

Table 1
Average Raman spectral characteristics of CM in the analyzed targets.

Spectrum name[a]	D pos. (cm^{-1})	D FWHM (cm^{-1})	G pos. (cm^{-1})	G FWHM (cm^{-1})	D/G intensity	2D pos. (cm^{-1})	2D FWHM (cm^{-1})	2D/G intensity
Bijiki BIF (TVA294-659.6)								
LL	1349.5	41.0	1578.2	22.6	0.07	2710.1	66.2	0.34
UL	1346.5	51.2	1576.5	25.5	0.12	2705.7	69.3	0.30
UR	1352.9	41.3	1581.1	23.9	0.33	2708.3	73.6	0.29
Vichadero BIF (050809l2)								
5i	1350.2	45.6	1579.7	25.7	0.18	2706.4	74.8	0.39
5i arrow	1348.4	37.0	1580.1	27.2	0.85	2697.3	51.0	1.31
5d	1351.3	45.4	1581.7	26.4	0.42	2705.8	74.8	0.46
5e	1347.5	53.2	1581.4	28.5	0.40	2705.3	75.1	0.36
5f	1345.7	45.2	1575.3	25.8	0.30	2703.4	72.3	0.30
5g	1345.3	45.5	1574.9	25.7	0.27	2702.5	73.9	0.31

[a] Spectrum names correspond to the images in Fig. 6.

and −15.5‰) but slightly lower carbon contents averaging 0.041 ± 0.041 wt% (1σ), which suggests that organic contamination was probably a source of carbon in untreated bulk powders. It is also possible that the loss of organic carbon during combustion at 550 °C was in part accelerated by reactions with oxidizing minerals in the Akilia Qp rock, as we noted that sulfides were converted to hematite during these experiments. Acidified muffled whole-rock powders had an average $\delta^{13}C_{gra}$ composition[1] of −17.5 ± 2.5‰ (1σ) and ranged between −12.6‰ and −23.6‰, which was isotopically lighter than untreated powders. Acidified muffled whole-rock powders contained an average graphite content of 0.008 ± 0.004 wt% (1σ), which represented between 0.16 and 1.81 μg of graphite. Therefore, multiple analyses of whole-rock powder aliquots showed minor heterogeneities in graphite abundances and isotope compositions. The isotopic composition of carbonate was measured in aliquots from the same sub-samples of whole-rock powders, which were found to have a range of $\delta^{13}C_{carb}$ composition[1] of −3.3‰ to −5.5‰ and an average $\delta^{18}O_{carb}$ composition[1] of −16.3 ± 0.3‰ (1σ). These carbon isotope compositions are similar to $\delta^{13}C_{carb}$ values from metacarbonates from the Isua Supracrustal Belt, which typically range between −4‰ and +2‰ (Naraoka et al., 1996; Ueno et al., 2002; and references therein).

Total carbon in untreated powders of the Vichadero BIF had an average $\delta^{13}C$ composition of −21.7 ± 2.0‰ (1σ) ($\delta^{13}C$ values between −19.4‰ and −23.2‰) for total carbon contents averaging 0.078 ± 0.041 wt% (1σ) (Table 2). Muffled aliquots of whole-rock powders were measured to have heavier $\delta^{13}C$ values with an average of −13.5 ± 2.4‰ (1σ) and significantly less total carbon average of

[1] The subscripts "gra" and "carb" for δ-values refer to graphite and carbonate, respectively.

Table 2
Stable isotope compositions of graphite and carbonate in differently processed whole-rock powders from the Akilia Qp rock and the two Paleoproterozoic BIFs.

Sub-sample[a]	Untreated WR powder		WR powder muffled at 550 °C for 2–4 h		Acidifed WR muffled powders			Carbonate analyses of WR rock powders			
	$\delta^{13}C_{TC}$ (‰)	% C	$\delta^{13}C_{TC}$ (‰)	% C	$\delta^{13}C_{org}$ (‰)	% C_{org}	$C_{analyzed}$ (μg)	$\delta^{13}C_{carb}$ (‰)	±1σ	$\delta^{18}O_{carb}$ (‰)	±1σ
G91-26AB	−5.4	0.151	−5.0	0.121	−15.7	0.004	0.16	−4.0	0.2	16.2	0.2
	−4.7	0.148	−4.6	0.117	−19.0	0.007	0.36				
	−5.6	0.149	−5.7	0.081	−17.3	0.005	0.54				
	−5.4	0.161			−17.5	0.005	0.45				
Average	−5.3	0.152	−5.1	0.106	−17.4	0.005					
SD	0.4	0.006	0.6	0.022	1.4	0.001					
G91-26CD	−17.8	0.069	−15.5	0.025	−17.3	0.010	0.54	−4.7	0.2	−16.1	0.1
	−17.4	0.066	−15.3	0.023	−16.6	0.007	0.41				
	−17.7	0.064	−13.8	0.014	−18.0	0.008	0.80				
	−17.1	0.057			−23.6	0.018	1.81				
Average	−17.5	0.064	−14.9	0.021	−18.9	0.011					
SD	0.3	0.005	0.9	0.006	3.2	0.005					
G91-26E	−8.6	0.036	−12.1	0.023	−19.2	0.010	0.53	−5.5	0.2	−16.8	0.2
	−12.1	0.038	−9.9	0.020	−18.5	0.008	0.43				
	−9.8	0.027	−7.8	0.008	−16.6	0.007	0.68				
					−16.2	0.006	0.53				
Average	−10.2	0.033	−9.9	0.017	−17.6	0.008					
SD	1.8	0.006	2.1	0.008	1.5	0.002					
G91-26F	−7.6	0.052	−11.4	0.026	−17.5	0.010	0.51	−3.3	0.3	−16.3	0.3
	−6.8	0.051	−8.3	0.021	−20.4	0.016	0.88				
	−9.7	0.051	−6.1	0.014	−12.6	0.005	0.53				
	−7.3	0.045			−13.9	0.006	0.60				
Average	−7.9	0.050	−8.6	0.021	−16.1	0.010					
SD	1.3	0.003	2.6	0.006	3.5	0.005					
Vichadero BIF											
50809/2	−22.4	0.084	−10.8	0.013	−33.6	0.010	2.99	−2.2	0.6	−13.5	0.4
	−23.2	0.116	−14.1	0.015	−25.8	0.011	1.94				
	−19.4	0.034	−15.4	0.014	−26.3	0.008	0.62				
Average	−21.7	0.078	−13.5	0.014	−28.6	0.010					
SD	2.0	0.041	2.4	0.001	4.4	0.002					
Bijiki BIF											
TVA294-659.6	−22.6	3.58	−21.1	3.22	−23.8	2.20	25.3	−14.9	0.1	−7.1	0.1
	−22.3	3.35	−23.2	2.83	−23.8	2.08	17.7				
	−22.5	3.49	−22.3	3.15	−24.3	2.87	21.0				
Average	−22.5	3.47	−22.2	3.07	−24.0	2.39					
SD	0.1	0.117	1.1	0.204	0.3	0.426					

[a] Several aliquots of the whole-rock powders were analyzed at least in triplicate.

0.014 ± 0.001 wt% (1σ), which is consistent with minor organic carbon infiltration from the modern environment or sample preparation. Acidified muffled whole-rock powders of the Vichadero BIF had an average $\delta^{13}C_{gra}$ composition of $-28.6 \pm 4.4‰$ (1σ) ($\delta^{13}C_{gra}$ values between $-25.8‰$ and $-33.6‰$) and an average of 0.010 ± 0.002 wt% (1σ) of graphite. Carbonate in the Vichadero BIF was measured to have a $\delta^{13}C_{carb}$ value of $-2.2‰$ and a $\delta^{18}O_{carb}$ value of $-13.5‰$.

Finally, untreated powders from the Bijiki BIF had an average $\delta^{13}C$ composition of $-22.5 \pm 0.1‰$ (1σ) for significantly more total carbon contents that averaged 3.5 ± 0.1 wt% (1σ) (Table 2). Muffled whole-rock powders from the Bijiki BIF had a similar average $\delta^{13}C$ composition of $-22.2 \pm 1.1‰$ (1σ), although slightly lower carbon abundances around 3.1 ± 0.2 wt% (1σ). Acidified muffled whole-rock powders had $\delta^{13}C_{gra}$ values around $-24.0‰$ and around 2.4 wt% graphite. Carbonate in the Bijiki BIF was measured to have a $\delta^{13}C_{carb}$ value of $-14.9‰$ and a $\delta^{18}O_{carb}$ value of $-7.1‰$.

4.2.2. Carbon isotope analyses of graphite from the Akilia Qp rock with the NanoSIMS

The instrumental mass fractionation (IMF) was observed to be similar for both graphite and diamond standards and carbon isotope analyses by NanoSIMS had a 2σ reproducibility of $1.8‰$ (Electronic Annex 7). Analyses of different graphite targets in the Akilia Qp rock were alternated with analyses of Sri Lanka graphite and 4139 diamond. Twenty-two analyses were performed on six graphite targets and had an average $\delta^{13}C_{gra}$ value of $-13.8 \pm 5.6‰$ (1σ), for a relatively large range of $\delta^{13}C_{gra}$ values between $-4.1‰$ and $-22.8‰$ (Table 3). The distribution of measured $\delta^{13}C_{gra}$ values was indistinguishable between graphite targets associated with apatite (average $= -13.0 \pm 6.7‰$ (1σ)) and those associated with hornblende or sulfides (average $= -13.8 \pm 5.6‰$ (1σ)) (Fig. 7). Secondary electron images of craters produced with the NanoSIMS after analysis (Electronic Annex 2) demonstrate the effective removal of significant quantities of graphitic material in the analyzed targets up to 3 μm below the surface of the polished section, and show that contributions from minor surface contamination were minimal.

4.3. Elemental composition of graphite

The presence and distribution of other elements, especially those of biological relevance, in graphite from the Akilia Qp rock were also analyzed with the NanoSIMS and compared semi-quantitatively with CM from Paleoproterozoic BIFs and fluid-deposited graphite. Compositional

Table 3
NanoSIMS analyses of graphite targets from G91-26.

Target/spot[a]	$^{13}C/^{12}C$[b]	Precision (%)	^{12}C counts	$\delta^{13}C$[c] (‰)
G91-26C 39 (graphite with apatite)				
1_2	1.1125E−02	9.68E−03	1.07E+10	−8.9
1_3	1.1068E−02	1.11E−02	1.13E+10	−14.0
1_4	1.0969E−02	1.37E−02	1.06E+10	−22.8
1_5	1.1088E−02	1.33E−02	9.91E+09	−12.2
1_6	1.1035E−02	1.24E−02	7.78E+09	−16.9
1_7	1.1052E−02	1.25E−02	9.26E+09	−15.4
G91-26C 44 (graphite with apatite)				
1_1	1.1018E−02	1.30E−02	1.08E+10	−18.4
1_2	1.1055E−02	1.64E−02	8.39E+09	−15.1
G91-26C 52 (graphite with hornblende + pyrrhotite)				
1_1	1.11654E−02	9.44E−03	1.27E+10	−5.3
1_3	1.1005E−02	1.39E−02	1.10E+10	−19.6
1_4	1.0985E−02	8.78E−03	1.73E+10	−21.4
G91-26C 57 (graphite with hornblende + pyrrhotite)				
1_1	1.1166E−02	9.12E−03	1.38E+10	−5.2
1_2	1.1178E−02	9.14E−03	1.23E+10	−4.1
1_3	1.1169E−02	1.08E−02	1.32E+10	−5.0
1_4	1.1061E−02	8.91E−03	1.37E+10	−14.6
1_5	1.1061E−02	9.21E−03	1.31E+10	−14.6
1_6	1.0975E−02	9.76E−03	1.60E+10	−22.2
1_7	1.1083E−02	8.47E−03	1.50E+10	−12.6
1_8	1.1021E−02	1.24E−02	1.25E+10	−18.2
1_9	1.1074E−02	8.72E−03	1.48E+10	−13.4
G91-26C 68 (graphite with apatite)				
1_1	1.1136E−02	1.26E−02	9.90E+09	−7.9
G91-26C 72 (graphite with apatite)				
1_1	1.1056E−02	1.83E−02	1.06E+10	−15.0

[a] Spot numbers are for different areas of the same graphite target.
[b] $^{13}C/^{12}C$ ratios are trend-corrected and corrected for IMF.
[c] 2σ reproducibility on δ-values is $1.8‰$.

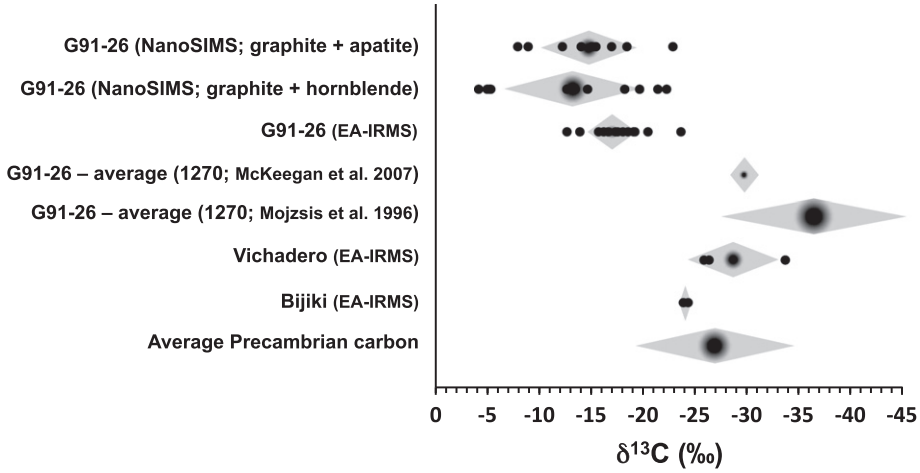

Fig. 7. Chart comparing $\delta^{13}C$ ranges for graphite in Akilia Qp rock sample G91-26 as measured with the NanoSIMS, EA-IRMS (on muffled and acidified whole-rock powders), and with the ims 1270 (Mojzsis et al., 1996; McKeegan et al., 2007). Gray diamonds show the 1σ range of $\delta^{13}C$ values with the darker center as the average. Data for muffled and acidified whole-rock powders from the Paleoproterozoic BIFs from Uruguay and Michigan are also shown and compared to the average ($\pm 1\sigma$) $\delta^{13}C$ value of Precambrian CM ($n = 1120$).

maps for graphite in the Akilia Qp rock showed trace amounts of heterogeneous levels of N, P, and S in graphite associated with apatite (Fig. 8a and b), and in graphite associated with hornblende (Fig. 8c and d) and calcite (Fig. 8e). Silicate phases surrounding the analyzed graphite targets were found to have less than 2 C/s (counts per second) of N, which is considered to be the background N level. Less than 1 C/s was measured for S and P in surrounding silicate and carbonate phases, but some S was detected in carbonate and apatite. Graphite in the Vichadero and Bijiki BIFs also contained trace abundances of these elements (Fig. 8f and g). An area around an apatite-associated carbonaceous target in the Bijiki BIF exhibited a gradient of secondary ions (increasing from right to left in the ^{16}O map of Fig. 8g), which was likely due to a slight topographic slope in this target. Secondary ionization of ^{12}C for dolomite was significantly lower than that for CM (Fig. 8g). Local surface variations and empty cracks or pits are probably responsible for the variable secondary ionization efficiency at grain boundaries with distinct orientations.

No significant differences in secondary ion counts were measured for graphite associated with apatite compared to graphite associated with calcite, hornblende, or pyrrhotite in the Akilia Qp rock (Electronic Annex 8). Nitrogen abundances in Akilia graphite were estimated by NanoSIMS to average 50 ± 47 ppm (1σ), which is similar to ranges reported for graphite from the Isua Supracrustal Belt and elsewhere (van Zuilen et al., 2005; Ader et al., 2006). Comparisons of relative secondary ion counts in CM showed generally decreasing H/C and O/C for CM from the Bijiki BIF ($H/C_{ave} = 0.22 \pm 0.12$ (1σ); $O/C_{ave} = 1.22 \pm 0.59$ (1σ)), the Vichadero BIF ($H/C_{ave} = 0.13 \pm 0.02$ (1σ); $O/C_{ave} = 0.52 \pm 0.21$ (1σ)), and the Akilia Qp rock ($H/C_{ave} = 0.05 \pm 0.04$ (1σ); $O/C_{ave} = 0.34 \pm 0.26$ (1σ)), consistent with the increasing metamorphic grades of these rocks (Fig. 9a). This trend, however, was not observed for N/C, P/C, and S/C, as CM from the Vichadero BIF had the lowest ratios (Fig. 9b and Electronic Annex 8). Fluid-deposited graphite from Mt. Kearsarge in New Hampshire was found to relatively high H/C (0.20), O/C (0.53) and N (600 ppm), while graphite from Sri Lanka had low H/C (0.01) and O/C (0.27) and relatively high N (176 ppm).

5. DISCUSSION

5.1. The origin of carbonaceous material in Paleoproterozoic BIFs

Apatite–graphite associations were common in the two metamorphosed Paleoproterozoic BIFs, which provides a suitable petrographic context to evaluate the origin of similar mineral associations in the Akilia Qp rock. During sedimentation and early diagenesis of BIFs, anaerobic heterotrophic oxidation of buried biomass can result in the liberation of phosphate and isotopically light bicarbonate into the sediment pore waters. These micro-environments then become host to the formation of ^{13}C-depleted diagenetic carbonate and phosphate minerals (e.g. Berner, 1990). Generations of such diagenetic processes were best illustrated in the Bijiki BIF, where early oxidation of sedimentary CM resulted in the accumulation of pore water carbonate and phosphate. Following the crystallization of the Fe-silicate matrix and subhedral magnetite grains (Fig. 4b and c), later diagenetic and metamorphic processes led to successive crystallization of apatite and euhedral magnetite, followed by the remobilization of carbonate into layers or veins (Fig. 4d–f). Based on petrographic observations from the Bijiki BIF, the amount of CM in post-depositional dolomite was generally less than in the Fe-silicate matrix, which suggests that CM had been more oxidized where carbonate was remobilized.

Raman spectra of graphite in the Bijiki BIF illustrate the impact of high-temperature metamorphism on the degree of ordering of CM and thereby confirm its indigenicity. The Bijiki BIF has a $\delta^{13}C_{org}$ value of $-24.0‰$ and a $\delta^{13}C_{carb}$ values around $-14.9‰$, which suggest that the dolomite incorporated a relatively high amount of diagenetically oxidized CM. Carbonaceous material in the Bijiki BIF also

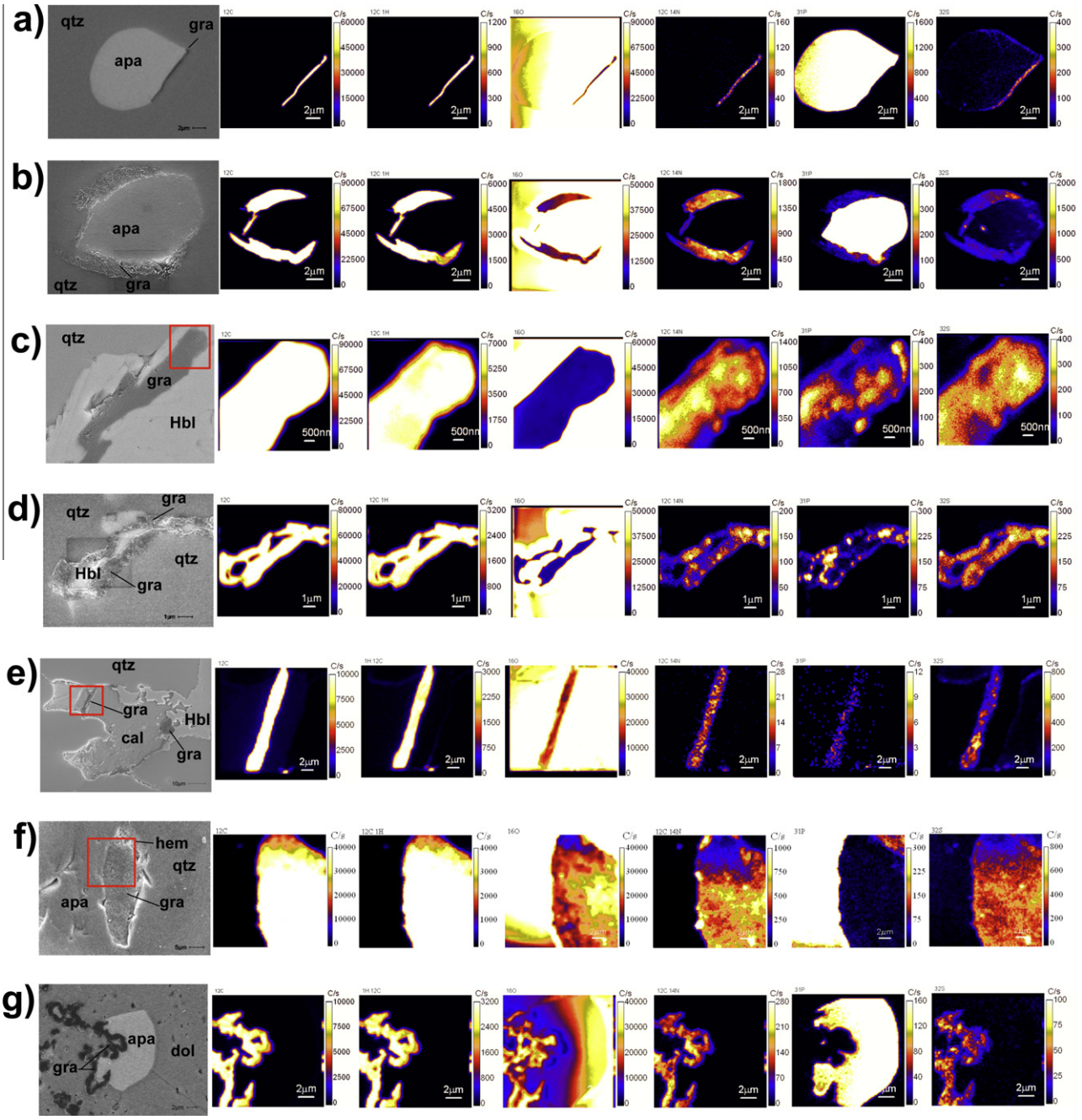

Fig. 8. Selected NanoSIMS elemental maps (of ^{12}C, $^{12}C^{1}H$, ^{16}O, $^{12}C^{14}N$, ^{31}P, and ^{32}S, from left to right) for graphite associated with apatite and other phases from (a–e) the Akilia Qp rock, (f) Vichadero BIF, (g) and Bijiki BIF. Secondary electron and BSE images show the context of the targets, count rates are shown for first-order comparisons, and mineral abbreviations are: apa, apatite; gra, graphite; hem, hematite; qtz, quartz; dol, dolomite; hbl, hornblende.

contained high levels of the elements C, H, N, O, P, and S (known hereafter as CHNOPS). During diagenesis and metamorphism, a fraction of these elements remains covalently bonded in CM of biological origin, but their relative abundances decreases with higher metamorphic grade (Strauss et al., 1992; Des Marais, 2001). These independent lines of evidence demonstrate the biogenic origin of CM in the Bijiki BIF and lead to the conclusion that diagenetic processes in sediments from the Baraga basin were fueled by intense primary productivity in the photic zone of the water column.

In the Vichadero BIF, many apatite grains and associated graphite were found in close proximity to hematite (Figs. 2c, d and 3e–h), which points to ferric iron remobilization and adsorption onto phosphate mineral surfaces during prograde metamorphism under conditions of high oxygen fugacity. Accordingly, either the phosphate was initially associated with settling ferric oxyhydroxide particles

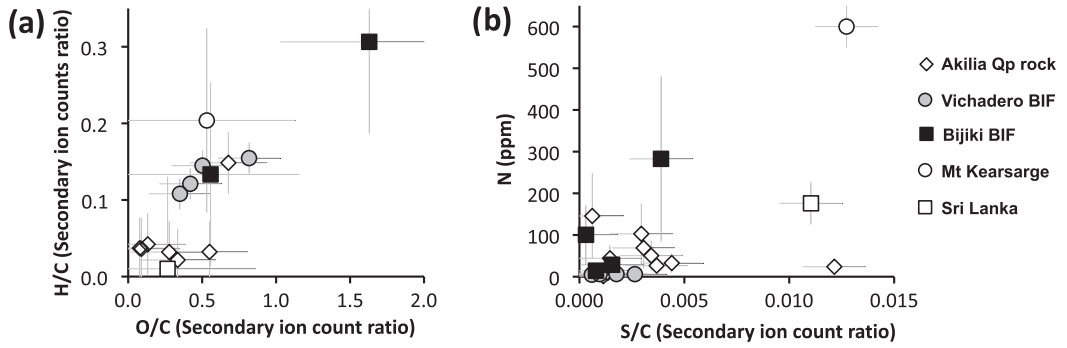

Fig. 9. Semi-quantitative plots of secondary ion ratios measured by NanoSIMS on various targets of CM from the Eoarchean Akilia Qp rock (G91-26), Paleoproterozoic BIFs from the Vichadero Formation (50809/2) and Bijiki member of the Michigamme Formation (TVA294-659.6), and graphite from Mount Kearsarge and from Sri Lanka comparing (a) $^{12}C^{1}H/^{12}C$ and $^{16}O/^{12}C$ and (b) N concentration (based on the measured $^{12}C^{14}N$ counts normalized to the average N from Mt. Kearsage and Sri Lanka graphites) and $^{32}S/^{12}C$ relative secondary ion counts. Errors are 70% for N abundance (except for Mt. Kearsage and Sri Lanka graphites, where it is around 50 ppm) and 1σ standard deviations for H/C, O/C, and S/C.

(Bjerrum and Canfield, 2002) or it was incorporated within the biomass of lysed planktonic cells (Konhauser et al., 2002, 2007). In either case, during diagenesis and prograde metamorphism, phosphate was released into porewaters, where supersaturation with respect to an apatite or a calcium fluorapatite precursor phase was achieved (Van Cappellen and Berner, 1988). The presence of quartz bands with several hundred apatite grains in the Vichadero BIF further suggests a diagenetic origin for such phosphatic layers and for apatite associations with graphite located therein. Similar to apatite-rich bands in the Bijiki BIF, apatite-rich bands in the Vichadero BIFs suggest that graphite associations with apatite are of diagenetic origin and can be preserved at metamorphic grades up to the upper amphibolite facies. However, while the origin of the Vichadero graphite likely formed from crystallization of sedimentary CM, fluid-deposition of this graphite may also be possible. Given that this BIF was deposited at a time when planktonic biomass was proliferating worldwide (e.g. Konhauser et al., 2005; Papineau, 2010), it is likely that it originally contained biogenic CM that underwent a series of post-depositional transformations.

Raman spectra of graphite associated with apatite exhibit a high degree of ordering consistent with a protracted metamorphic history. The Vichadero BIF has an average $\delta^{13}C_{gra}$ value of $-28.6‰$ and $\delta^{13}C_{carb}$ values around $-2.2‰$, which suggest that the carbonate solid-phase did not incorporate a large amount of diagenetically oxidized organic matter. Instead, negative $\delta^{13}C_{carb}$ values in highly metamorphosed rocks may be due to ^{13}C-depletions from diagenetic carbonate, but could also have arisen from high-temperature devolatilization reactions that leave residual carbonate more depleted in ^{13}C (Deines and Gold, 1969; Lattanzi et al., 1980; Valley, 1986; Kaufman, 1996; DesMarais, 2001). Carbonaceous material in the Vichadero BIF generally contained lower levels of the CHNOPS elements compared to CM from the Bijiki BIF (Fig. 9 and Electronic Annex 8), which suggests higher losses from metamorphic devolatilization. However, despite different metamorphic histories, the relative abundances of P and S were similar, which is analogous to what has been observed in the CM-rich Gunflint and Apex cherts, in which the relative abundances of N, S, and P were found to be similar despite differences in provenance and metamorphic grade (De Gregorio et al., 2009). These various lines of evidence collectively suggest a biogenic origin for CM in the Vichadero BIF.

5.2. Graphite and carbonate in the Akilia Qp rock

Graphite in the Akilia Qp rock occurred as discrete coatings on apatite grains and in complex mineral assemblages that included hornblende ± calcite ± magnetite ± pyrrhotite ± chalcopyrite, with occasional micrometer-size pentlandite zones (Papineau et al., 2010). These petrographic observations suggest, that some of the graphite in the Akilia Qp rock was fluid-deposited at high-temperature during metamorphism. The range of $\delta^{13}C_{gra}$ values for acidified muffled whole-rock powders was found by EA-IRMS to be between $-12.6‰$ and $-23.6‰$ and is interpreted to represent centimeter-scale carbon isotope heterogeneities. The total graphite content of the Akilia Qp rock averaged 0.008 wt% and was similar to that measured in the Vichadero BIF, although the Akilia graphite was less ^{13}C-depleted. Such low levels of organic carbon are common in BIFs with dominant oxide or siderite mineralogy, which typically contain between 0.01 and 0.20 wt% organic carbon (Klein, 2005).

The range of $\delta^{13}C_{gra}$ values measured with the NanoSIMS was indistinguishable for graphite associated with apatite compared to graphite associated with hornblende and other minerals (Fig. 7), which suggests a common carbon source. These analyses of the Akilia graphite revealed $\delta^{13}C_{gra}$ values between $-4.1‰$ and $-22.8‰$, which are in broad agreement with the carbon isotope measurements from the EA-IRMS and represent carbon isotope heterogeneities at micron scales. Similar large ranges of isotopically heavy graphite have been reported from metacherts, schists, and metacarbonate rocks of the Isua Supracrustal Belt, where the $\delta^{13}C_{gra}$ values measured by SIMS varied between

−18‰ and +2‰ (Ueno et al., 2002). The latter SIMS analyses further revealed that graphite inclusions in garnet and quartz are more ^{13}C-depleted (by up to 7‰) compared to graphite located along mineral grain boundaries, which was interpreted as the result of mineral armoring of less altered graphite inclusions. It was then concluded that isotope exchanges with carbon-bearing fluids during regional metamorphism at Isua led to increased $\delta^{13}C_{gra}$ values compared to precursor CM, possibly of biological origin (Ueno et al., 2002). In the Akilia Qp rock, carbon isotope heterogeneities occur at various scales and may be related to precipitation from a fluid that was isotopically fractionated during Rayleigh-type distillation.

To test this hypothesis, we modeled the formation of graphite from CO_2- and CH_4-bearing metamorphic fluids (Naraoka et al., 1996). Calculations were made using a batch model with the assumptions that graphite continuously formed from CO_2 and CH_4 in equal proportions and that small amounts of graphite are progressively precipitated in constant isotopic equilibrium with the CO_2–CH_4 fluid. Isothermal reactions were calculated with temperature estimates (between 635 and 830 °C) based on Raman spectral parameters of Akilia graphite (Papineau et al, 2010). Changes in $\delta^{13}C^{i}_{fluid}$ were assumed to follow the Rayleigh distillation equation (1) and the $\delta^{13}C^{f}_{graphite}$ value for accumulated graphite was calculated from a mass-balance equation (2):

$$\delta^{13}C^{f} = (\delta^{13}C^{i} + 1000) \times f^{\alpha-1} - 1000 \quad (1)$$

$$\delta^{13}C^{i}_{fluid} = (\delta^{13}C^{f}_{fluid} \times f + \delta^{13}C^{f}_{graphite} \times (1-f) \quad (2)$$

where f is the fraction of residual carbon in the fluid and α is the equilibrium fractionation factor at a given temperature. The initial input parameter in the model for the $\delta^{13}C^{i}_{CO_2}$ value was −4.0‰ (assumed to be in equilibrium with the measured $\delta^{13}C_{carb}$ in the Akilia Qp rock) and the $\delta^{13}C^{i}_{CH_4}$ was calculated from the equilibrium isotopic fractionation factor between CO_2 and CH_4 (Ohmoto and Rye, 1979). Results from these calculations (Fig. 10a and b) suggest that graphite produced from such fluids could have $\delta^{13}C_{gra}$ values around −11.5‰ (with f between 1 and 0.5 and at $T = 635$ °C) or $\delta^{13}C_{gra}$ values around −7‰ (with f between 0.7 and 0.3 and at $T = 830$ °C), which are consistent with some carbon isotope compositions measured by NanoSIMS. Alternatively, the $\delta^{13}C_{fluid}$ value could have been changing in composition with different carbon sources mixing during precipitation. However, to explain the more depleted $\delta^{13}C$ values another model may be necessary.

In this work, two independent methods for carbon isotope analysis of graphite have revealed consistent results that are significantly different from published compositions. In fact, previous SIMS measurements revealed a large range of $\delta^{13}C_{gra}$ values between −21‰ and −49‰ for asserted graphite inclusions in apatite in Akilia Qp rock sample G91-26 (Fig. 7; Mojzsis et al., 1996). McKeegan et al. (2007) independently performed two analyses of asserted graphite inclusions in apatite from this same sample and obtained $\delta^{13}C_{gra}$ values of -29.7 ± 1.3‰ (1σ), using the same technique and instrument. Since independently measured $\delta^{13}C_{gra}$ values of graphite coatings on apatite with the NanoSIMS and bulk graphite by EA-IRMS both

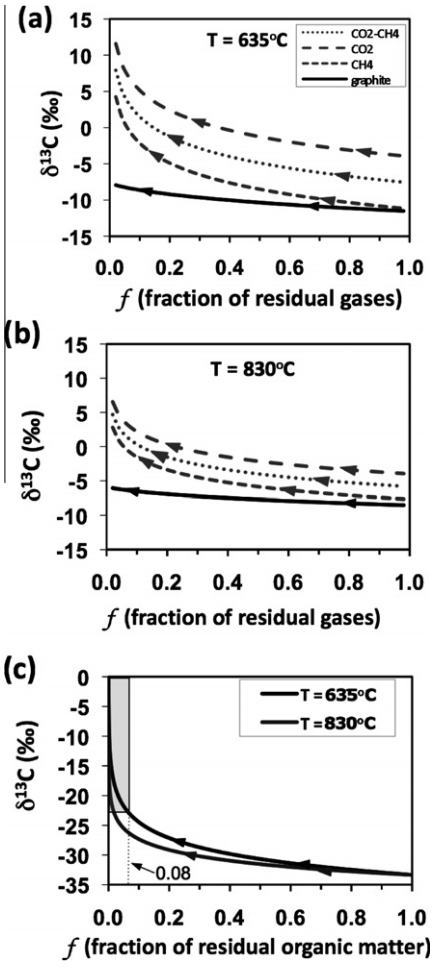

Fig. 10. Models of the $\delta^{13}C$ composition of graphite formed by precipitation from mixed CO_2- and CH_4-bearing fluids in a closed system at temperatures (a) of 635 °C and (b) of 830 °C, and (c) the progressive loss of hydrocarbons from carbonaceous material, assuming an initial $\delta^{13}C^{i}$ of −33.4‰. The f values are the molar ratios of the residual organic carbon to the initial organic carbon content.

revealed heavier values and heterogeneities at various scales, the difference in the analytical spot size (4 μm with the NanoSIMS versus 30 μm with the ims 1270) is an unlikely explanation for the difference in isotope composition.

Variable metamorphic imprints on isotopic compositions of micro-domains may explain some differences in the datasets, since metamorphism is expected to affect $\delta^{13}C_{gra}$ values by driving them towards heavier values. A Rayleigh distillation model is used to estimate changes in carbon isotope composition during metamorphic devolatilization and/or isotope exchanges with carbonate. While sensu stricto graphite inclusions in apatite have yet to be documented within cross-sectional focused ion beam lift-out sections in the Akilia Qp rock, it has been argued that armoring of CM by apatite would minimize isotopic fractionation during metamorphism (Mojzsis et al., 1996; Eiler et al., 1997). Therefore, a Rayleigh-type distillation mechanism would have preferentially affected the carbon isotope composition of graphite coatings (as measured in this work)

compared to asserted graphite inclusions in apatite (as measured by Mojzsis et al., 1996; McKeegan et al., 2007). Such a model was calculated using Eq. (1) for two equilibrium fractionation factors (for $T = 635$ and 830 °C and α calculated from Deines and Eggler, 2009) and is presented in Fig. 10c. The $\delta^{13}C^{i}$ value was taken to be $-33.4‰$ or the average of data from Mojzsis et al. (1996) and McKeegan et al. (2007) for graphite completely armored by apatite. Our calculations suggest that $\delta^{13}C_{gra}$ values up to $-23‰$ can be achieved after the loss of 92% of the original carbonaceous material ($f = 0.08$, $T = 635$ °C) from Rayleigh-type distillation processes. Since the average content of graphite in the Akilia Qp is around 0.009 wt%, this calculation predicts that the original amount of CM in this rock could have been up to 0.11 wt%. If this model correctly reflects the distribution of graphite in the Akilia Qp rock, then the bulk graphite is significantly more abundant and less ^{13}C-depleted than the asserted graphite inclusions in apatite. We emphasize, however, that the presence of sensu stricto graphite inclusions in Akilia apatites remains to be unambiguously documented in FIB lift-out sections (Papineau et al., 2010). While this Rayleigh distillation model may be consistent with published data, it is unclear whether differences in measurement techniques played a role in the differences between our NanoSIMS measurements of graphite targets exposed at the thin section surface and SIMS measurements by Mojzsis et al. (1996) and McKeegan et al. (2007) of graphite targets from below the thin section surface by sputtering away the overlying material.

The average of bulk $\delta^{13}C$ compositions of calcite and graphite in the Akilia Qp rock are $-4.4‰$ and $-17.5‰$, respectively, which indicates that these minerals did not reach isotopic equilibrium and formed from distinct sources of carbon-bearing compounds. In fact, experimental calibration of the carbon isotope equilibrium fractionation factor for graphite and calcite at temperatures relevant to graphitization in the Akilia Qp rock (e.g. 750 °C) predicts that the difference in $\delta^{13}C$ values should be around $3‰$ (Deines and Eggler, 2009). Carbonate minerals commonly occur in BIFs and are often characterized by negative $\delta^{13}C_{carb}$ values (Klein, 2005). The isotope composition of bulk calcite in the Akilia Qp rock may reflect (1) small ^{13}C-depletions from the preferential devolatilization of $^{13}CO_2$ during metamorphic decarbonation reactions (Deines and Gold, 1969; Lattanzi et al., 1980), (2) carbon isotope exchange with the isotopically light graphite or precursor CM, (3) mantle sources of CO_2 in infiltrating fluids, or (4) a combination of these factors.

5.3. Comparison between the Akilia Qp and younger rocks

5.3.1. Graphite associated with apatite

Clues to the origin of apatite + graphite associations in the granulite facies Akilia Qp rock may be provided by the petrographic context from the two studied Paleoproterozoic BIFs that were metamorphosed at the amphibolite to upper amphibolite facies. However, the petrographic distribution of graphite in the Bijiki BIF was generally different from that in the Vichadero BIF and in the Akilia Qp rock. The organic-rich Bijiki BIF contained graphitic filaments throughout its matrix and sometimes formed dense layers of carbonaceous material, which were not observed in the other studied samples. Graphite coatings and inclusions (sensu stricto) in apatite grains were most abundant in this rock (around 78% of apatite grains), but apatite grains occurred in bands and veins of diagenetic dolomite. For comparison, graphite in the organic-poor Vichadero BIF was only found to occur in association with apatite in quartz bands. These apatite grains contained fewer graphite coatings (only about 5% of apatite grains) and were often associated with hematite and calcite. These observations collectively demonstrate: (1) that apatite grains in the analyzed metamorphosed BIFs often form bands parallel to bedding; (2) that CM is frequently associated with apatite grains in BIFs; (3) that the proportion of these mineral associations is related to the total amount of organic matter in the rock; (4) that a series of biogeochemical processes beginning with the concentration of phosphate during diagenesis can eventually lead to the association of apatite with CM in Paleoproterozoic BIFs; and (5) that diagenetic mineral associations between apatite and graphite can survive high-grade metamorphism, at least up to the amphibolite facies.

In the Akilia Qp rock, graphite occurred in complex mineral assemblages and also as thin coatings on discrete apatite grains (about 18% of apatite grains) typically located in quartz-rich bands (Papineau et al., 2010). While the Akilia graphite + apatite associations possibly had a diagenetic origin, the fluid-deposition of such mineral associations from high-temperature fluids containing CM and phosphate is also possible but remains to be demonstrated. Therefore, the simple metamorphic recrystallization of diagenetic apatite + graphite associations may not accurately describe the complex pathways of phosphate and CM in the Akilia Qp rock.

5.3.2. Curled graphite structures in highly metamorphosed rocks

Raman microspectroscopic imaging of the Vichadero BIF revealed a graphite target that contained a 1 μm unique graphite structure, identified by an unusually strong 2D-band around 2700 cm^{-1} (arrowed in Fig. 5i). This structure was similar to curled graphite structures interpreted in the Akilia Qp rock (Papineau et al., 2010), although its Raman spectrum (Fig. 6) differed from that of the Akilia sample in that it had a significantly more intense D-band. Such spectral features may be attributed to the presence of a partially disordered curled graphite structure or partially hydrogenated graphene sheets (Elias et al., 2009; Papineau et al., 2010). Graphite "whisker" structures with similar Raman spectra are known to form during high-temperature experiments (Tan et al., 2001), but it is unclear if the experimental conditions under which graphite whiskers form are applicable to these geological settings. Nevertheless, these high-temperature experiments suggest that the graphite in the Vichadero BIF formed during a high-temperature event, most likely at the peak metamorphic temperature experienced by this rock. Apatite-associated graphite with spiral and conical structures has been documented by Raman spectroscopy and secondary electron

microscopy in a mineralogically complex graphite-bearing alkaline pegmatite from the Kola Peninsula in northwest Russia (Jaszczak et al., 2007). While this rock is igneous in origin, its carbon is ^{13}C-depleted and was interpreted by Jaszczak et al. (2007) to be biogenic in origin. The curled graphite structures found in the Vichadero BIF and the Akilia Qp rock are consistent with their high metamorphic grades, at the upper amphibolite and granulite facies respectively, but the minimum temperature and formation conditions at which these structures can form remains unknown.

5.3.3. Isotope compositions

The carbon isotope composition of CM is susceptible to fractionation during thermal breakdown and aromatization of organic molecules and is predicted to gradually become less ^{13}C-depleted with increasingly elevated metamorphic regimes (Hayes et al., 1983). At the amphibolite to granulite facies, residual CM can become ^{13}C-enriched by several permil and therefore the $\delta^{13}C_{gra}$ values presented in this work represent maximum values of their pre-metamorphic CM, whatever its origin. The protracted metamorphic history of the Akilia Qp rock included several high-temperature events that may be partly responsible for the large range of $\delta^{13}C_{gra}$ values (Fig. 7) and these carbon isotope compositions were more ^{13}C-depleted before metamorphism. While the smaller ranges of isotopically lighter $\delta^{13}C_{gra}$ values for the Vichadero and Bijiki BIFs are similar to typical Precambrian CM, these values are also likely to have been similarly affected by metamorphism.

Unlike the highly ^{13}C-depleted diagenetic dolomite from the Bijiki BIF, the Akilia Qp rock and the Vichadero BIF have been more highly metamorphosed and therefore, it is not possible to determine whether their slightly negative $\delta^{13}C_{carb}$ values are due to ^{13}C-depletions from diagenetic carbonate, high-temperature devolatilization reactions, or both. Similarly to carbonate carbon isotope systematics, $\delta^{18}O_{carb}$ values also decrease with higher metamorphic grades (Valley, 1986; Kaufman, 1996). Indeed, calcite from the Akilia Qp rock was the most ^{18}O-depleted, followed by calcite in the Vichadero BIF and dolomite from the Bijiki BIF (Table 2), which is consistent with progressively lower metamorphic grades for these rocks.

5.3.4. Trace elements abundances in graphite

Published NanoSIMS observations of Neoproterozoic filamentous microfossils suggest that some of the CHNOPS elements can be preserved and heterogeneously distributed within biogenic CM (Oehler et al., 2006). This approach has also been applied to organic particles and filaments in Archean quartzites and cherts, where various elements correlate with CM exposed at the surface of thin sections (Wacey et al., 2008; Oehler et al., 2009). However, elemental imaging with the NanoSIMS typically requires a primary ion beam of only a few pA, which removes only a few nanometers thickness of sample material. Extreme care must therefore be taken in the preparation and pre-characterization of samples to reduce surface contamination. Sources of contamination for H, N, O, P, and S can be minimized by avoiding the use of immersion oil on the thin section and by taking precautions during polishing and storage. In addition to these preventive measures, our samples were ion-milled with Ar^+ prior to gold coating. Nanometer-scale layers of amorphous carbon are also expected to be present on top of the gold coat during SEM observations prior to analyses with the NanoSIMS and while most of this was likely removed during pre-sputtering, non-quantified amounts of this contaminant may have been implanted into the targets during analyses. However, this possible source of contamination was very small because it would result in unstable secondary ion counts over several tens of cycles, which were not observed.

The CHNOPS elements were observed to occur in all targets of graphite whether from the Akilia Qp rock, the Paleoproterozoic BIFs of Uruguay and Michigan, or from fluid-deposited graphite (Fig. 8). The elements H and O were found to occur in slightly greater abundance in CM associated with apatite from the Paleoproterozoic Vichadero and Bijiki BIFs, although similar ranges of S and N were measured in most targets (Fig. 9 and Electronic Annex 8). However, it is unclear whether the observed heterogeneities relate to the distribution of N, P, and S within graphite or to nano-scale topographic variations in the polished and subsequently Ar-milled graphite surfaces. The presence and similar relative abundance of the CHNOPS elements in various graphite targets from the Akilia Qp rock further suggest a common carbon source for the Akilia graphite. Lower relative abundances of H and O compared to younger BIFs are also consistent with a stronger imprint of metamorphism on precursor CM, although differences in precursor material cannot be ruled out. Similarly, the local bonding environment of the CHNOPS elements in the Akilia graphite remains undetermined as they could either be incorporated into aromatic heterocycles or intercalated between graphite sheets, possibly from diffusion in graphite during metamorphism or metasomatism, and therefore later non-indigenous introduction of these elements into graphite is also plausible. The high sensitivity of the NanoSIMS allowed for the detection of the CHNOPS elements, whereas their trace levels were too low to be detected by energy dispersive spectroscopy in the TEM or by synchrotron-based scanning transmission X-ray microscopy (Papineau et al., 2010). Although abiogenic sources of CM produced from Fischer–Tropsch type reactions or siderite decarbonation are not predicted to contain N, S, or P, it is possible that abiogenic hydrothermal synthesis of organic compounds from simple precursors could have produced CM with structural S and N (Rushdi and Simoneit, 2004, 2005).

5.4. Implications for graphitization in the Akilia Qp rock

Apatite + graphite associations are not known to arise from unambiguously abiogenic processes and the only documented occurrences in an igneous rock are from a mineralogically complex graphite-bearing alkaline pegmatite, from the Kola Peninsula in northwest Russia (Jaszczak et al., 2007). In fact, the nature and mode of occurrence of graphite in this rock of enigmatic origin were interpreted to indicate a fluid-deposited origin, while its average $\delta^{13}C_{gra}$ composition of $-15.1‰$ was used to suggest mixing

between biogenic and carbonate-derived carbon (Jaszczak et al., 2007). Examples of granulite facies rocks that contain graphite deposited from CO_2- and CH_4-containing fluids that sourced a mixture of CM from mantle or the host metasedimentary rocks, or both, include quartz-monzonites and paragneisses from Mount Kearsage in New Hampshire (Rumble and Hoering, 1986; Rumble et al., 1986) and charnockite dykes and paragneisses from Sri Lanka (Farquhar and Chacko, 1991; Farquhar et al., 1999). Fluid-deposited graphites from New Hampshire and Sri Lanka have large ranges of $\delta^{13}C_{gra}$ values between −25‰ and −9‰ and between −23.4‰ and −7.5‰, respectively, which were interpreted to reflect different generations of graphite formation and fluid infiltration with variable mixtures of CH_4 and CO_2 (Rumble et al., 1986; Farquhar et al., 1999). These graphites also contain the CHNOPS elements (Fig. 9 and Electronic Annex 8), which further supports the interpretation that their parent CO_2 and CH_4 fluids partly sourced biogenic CM from nearby metasedimentary rocks.

Petrographic evidence shows that some of the Akilia graphite was fluid-deposited under high-temperature conditions (Papineau et al., 2010). Since this graphite essentially has the same range of $\delta^{13}C_{gra}$ values as graphite associated with apatite and also contains similarly high abundances of trace elements, we conclude that all the Akilia graphite formed from the same source(s) of CM. The Akilia graphite is also significantly ^{13}C-depleted, compared to co-occurring calcite, and it preserves elemental distributions that may have partly originated from decayed biogenic CM. Accordingly, there may have been several generations of graphite formation along with possibly varying mixtures and sources of CO_2- and CH_4-bearing fluids that resulted in the large range of $\delta^{13}C_{gra}$ values. In metacarbonate rocks that contain graphite associated with siderite and magnetite, the disproportionation of ferrous carbonate has been invoked to explain the origin of graphite (van Zuilen et al., 2002). However, since carbon isotope fractionation factors for graphite formed from such decarbonation reactions have yet to be determined experimentally, and because siderite has not been found in association with graphite in the Akilia Qp rock, this process cannot unambiguously explain our observations. The possibility of fluid-deposition of associated graphite and apatite in BIFs should be the focus of future investigations.

6. CONCLUSIONS

Detailed petrographic observations of apatite in two Paleoproterozoic BIFs show that diagenetic apatites often form bands parallel to bedding and are frequently associated with CM, depending on the total organic contents of the rock. A series of biogeochemical processes beginning during diagenesis can eventually lead to the association of apatite with biogenic CM in Paleoproterozoic BIFs and these mineral associations can survive high-grade metamorphism, at least to the amphibolite facies. Apatite-associated graphite in the Akilia Qp rock may have formed from a series of (bio)-geochemical processes similar to those inferred for Paleoproterozoic BIFs, but ambiguities remain in the case of such ancient rocks.

Graphite from the Akilia Qp rock has a wide range of carbon isotope compositions and two independent methods were used to measure the range of $\delta^{13}C$ values of graphite in the Akilia Qp rock. Analyses by EA-IRMS on acidified muffled whole-rock powders revealed $\delta^{13}C_{gra}$ values between −12.6‰ and −23.6‰, whereas analyses by NanoSIMS revealed values between −4.1‰ and −22.8‰, which is significantly less ^{13}C-depleted than the data of Mojzsis et al. (1996) and McKeegan et al. (2007). Because metamorphism at the amphibolite to granulite facies leads to increases in $\delta^{13}C_{gra}$ values, the most ^{13}C-depleted values likely represent the maximum $\delta^{13}C_{gra}$ values of the pre-metamorphic CM, and the large ranges measured may be partly attributed to variable carbon isotopic exchanges with metamorphic fluids. Models based on Rayleigh-type distillation suggest that graphite deposited from fluids with varying mixtures of CO_2 and CH_4 could have $\delta^{13}C$ values down to −11.5‰, which is consistent with a portion of the measured carbon isotope compositions. It is unclear whether differences in measurement techniques played a role in the significant differences between our NanoSIMS measurements of graphite targets exposed at the thin section surface and SIMS measurements by Mojzsis et al. (1996) and McKeegan et al. (2007) of asserted graphite inclusions from below the thin section surface by sputtering away the overlying material. Rayleigh-type distillation processes could have yielded graphite with $\delta^{13}C$ values down to −23‰ from precursor biogenic CM with an initial $\delta^{13}C$ value around −33‰, if more than 92% of the original CM was lost during metamorphic devolatilization reactions. If this model is correct, then the bulk graphite is significantly more abundant and less ^{13}C-depleted than the asserted graphite inclusions. To test this model however, the presence of sensu stricto graphite inclusions in Akilia apatites must be unambiguously documented.

A plausible mechanism for graphitization in the Akilia Qp rock was fluid-deposition under high-temperature conditions in association with the co-precipitation of other phases including calcite and ferruginous minerals (Papineau et al., 2010). This mechanism may also apply for graphite associated with apatite, although the direct crystallization of diagenetic CM associated with apatite cannot be entirely excluded for the Akilia Qp rock. Sources of carbon for the inferred CO_2 and CH_4 fluids in the Akilia Qp rock may have included both mantle gases and decayed biological CM. This possibility is substantiated by the presence of the CHNOPS elements in the Akilia graphite associated with apatite and with ferruginous mineral assemblages that often include calcite. Heteroatom abundances in Akilia graphite are also generally slightly lower than those observed in CM from Paleoproterozoic BIFs. More detailed petrographic and geochemical analyses are needed to assess whether CM associations with apatite reported from Eoarchean metacarbonate rocks from Isua (van Zuilen et al., 2002, 2005; Lepland et al., 2002) may indeed involve biogenic sources of carbon.

Collectively our results do not exclude a biogenic origin of the carbon in the Akilia graphite, but because some observations do not exclude graphitization of abiogenic carbon from fluid-deposition, ambiguities remain for the

exact origin(s) of this ancient carbon. Specifically, the deposition of graphite associations with apatite from high-temperature fluids containing CM and phosphate is possible but remains to be documented. Combined with data presented in Papineau et al. (2010), this study provides unprecedented details of the nature of graphite in the Eoarchean Akilia Qp rock, that can be used to compare with other metasedimentary rocks with complex metamorphic histories. This study lays the foundations for further investigations in a wider variety of samples and may eventually lead to the discovery of Earth's earliest biologically-derived carbon. The correlated use of multiple micro-analytical techniques has been successfully applied to provide several independent proxies to trace carbon pathways in highly metamorphosed sedimentary rocks and this multi-disciplinary approach is ideally suited to study carbonaceous particles from other complex geological environments elsewhere in the Solar System.

ACKNOWLEDGEMENTS

We would like to thank L. Nittler and E. Hauri for discussions on data acquired with the NanoSIMS and R. Bowden for help with some analyses by IRMS. Discussions with D. Rumble, R. Hazen, B. French, and T. McCollom helped to improve an early version of the manuscript. C. House kindly provided a graphite powder standard used in this work. We would like to thank M. Humphrey and A. Aibak for assistance in the Marquette drill core library and the Geological Survey of Michigan for granting access. Three anonymous reviewers are gratefully acknowledged for thoughtful comments that greatly improved the manuscript. We gratefully acknowledge funding from the NASA Exobiology and Evolutionary Biology Program (Grant No. NNX08AO16G), the NASA Astrobiology Institute (Grant No. NNA04CC09A), and the W.M. Keck Foundation. D.P. is very grateful for continuing financial support from the Geophysical Laboratory of the Carnegie Institution of Washington, Carnegie of Canada, the NAI, and the Fond québécois de la recherche sur la nature et les technologies. K.K. acknowledges funding through a NSERC Discovery Grant.

APPENDIX A. SUPPLEMENTARY DATA

Supplementary data associated with this article can be found, in the online version, at doi:10.1016/j.gca.2010.07.002.

REFERENCES

Ader M., Cartigny P., Boudou J.-P., Oh J. H., Petit E. and Javoy M. (2006) Nitrogen isotopic evolution of carbonaceous matter during metamorphism: methodology and preliminary results. *Chem. Geol.* **232**, 152–169.

André L., Cardinal D., Alleman L. Y. and Moorbath S. (2006) Silicon isotopes in <3.8 Ga West Greenland rocks as clues to the Eoarchaean supracrustal Si cycle. *Earth Planet. Sci. Lett.* **245**, 162–173.

Bernard S., Beyssac O. and Benzerara K. (2008) Raman mapping using advanced line-scanning systems: geological applications. *Appl. Spectrosc.* **62**, 1180–1188.

Berner R. A. (1990) Diagenesis of phosphorus in sediments from non-upwelling areas. In *Phosphate Deposits of the World: Neogene to Modern Phosphorites*, vol. 3 (eds. W. C. Burnett and S. R. Riggs). Cambridge University Press, Cambridge, pp. 27–32.

Beyssac O., Goffe B., Chopin C. and Rouzaud J. N. (2002) Raman spectra of carbonaceous material in metasediments: a new geothermometer. *J. Met. Geol.* **20**, 859–871.

Bjerrum C. J. and Canfield D. E. (2002) Ocean productivity before about 1.9 Gyr ago limited by phosphorus adsorption onto iron oxides. *Nature* **417**, 159–162.

Bolhar R., Kamber B. S., Moorbath S., Fedo C. M. and Whitehouse M. J. (2004) Characterisation of early Archaean chemical sediments by trace element signatures. *Earth Planet. Sci. Lett.* **222**, 43–60.

Cordani U. G. and Solani, Jr., E. (1990) Idades K–Ar e Rb–Sr das "Ilhas Cristalinas" de Rivera e Acegua (Uruguai e Rio Grande do Sul, Brasil) e seu enquadramento no contexto geotectonico regional. *An. Acad. Bras. Cienc.* **62**, 145–156.

Dauphas N., Van Zuilen M., Wadhwa M., Davis A. M., Marty B. and Janney P. E. (2004) Clues from Fe isotope variations on the origin of early Archean BIFs from Greenland. *Science* **306**, 2077–2080.

Dauphas N., van Zuilen M., Busigny V., Lepland A., Wadhwa M. and Janney P. E. (2007) Iron isotope, major and trace element characterization of early Archean Supracrustal rocks from SW Greenland: protolith identification and metamorphic overprint. *Geochim. Cosmochim. Acta* **71**, 4745–4770.

De Gregorio B. T., Sharp T. G., Flynn G. J., Wirick S. and Hervig R. (2009) Biogenic origin for Earth's oldest putative microfossils. *Geology* **37**, 631–634.

Deines P. and Gold D. P. (1969) The change in carbon and oxygen isotopic composition during contact metamorphism of Trenton limestone by the Mt. Royal pluton. *Geochim. Cosmochim. Acta* **23**, 421–424.

Deines P. and Eggler D. H. (2009) Experimental determination of carbon isotope fractionation between $CaCO_3$ and graphite. *Geochim. Cosmochim. Acta* **73**, 7256–7274.

DesMarais D. (2001) Isotopic evolution of the biogeochemical carbon cycle during the Precambrian. In *Stable Isotope Geochemistry*, vol. 43 (eds. J. W. Valley and D. R. Cole). Mineralogical Society of America, Washington, DC, Rev. Mineral. Geochem., pp. 555–578.

Eiler J. M., Mojzsis S. J. and Arrhenius G. (1997) Carbon isotope evidence for early life. *Nature* **386**, 665.

Elias D. C., Nair R. R., Mohiuddin T. M. G., Morozov S. V., Blake P., Halsall M. P., Ferrari A. C., Boukhvalov D. W., Katsnelson M. I., Geim A. K. and Novoselov K. S. (2009) Control of graphene's properties by reversible hydrogenation: evidence for graphene. *Science* **323**, 610–613.

Ellis J. H. (1998) The Precambrian supracrustal rocks of the "Isla Cristalina de Rivera" in northern Uruguay and their ore deposits: definition of a new lithostratigraphic unit ("Vichadero Formation") and a contribution to the genesis of banded iron-formation and manganese-formation. *Heidelberger geowissenschaftliche Abhandlungen: Band 90*, 196p.

Farquhar J., Hauri E. and Wang J. (1999) New insights into carbon fluid chemistry and graphite precipitation: SIMS analysis of granulite facies graphite from Ponmudi, South India. *Earth Planet. Sci. Lett.* **171**, 607–621.

Farquhar J. and Chacko T. (1991) Isotopic evidence for involvement of CO_2-bearing magmas in granulite formation. *Nature* **354**, 60–63.

Fedo C. M. and Whitehouse M. J. (2007) Do iron isotopes require a BIF origin for quartz-pyroxene rocks on Akilia, SW Greenland? *Geol. Soc. Am. Abstr. Programs 39*, p. 409.

Fedo C. M., Whitehouse M. J. and Kamber B. S. (2006) Geological constraints on detecting the earliest life on Earth: a perspective

from the Early Archaean (3.7 Ga) of Southwest Greenland. *Philos. Trans. R. Soc. Lond. B* **361**, 851–867.

Fedo C. M. and Whitehouse M. J. (2002a) Metasomatic origin of quartz-pyroxene rock, Akilia, Greenland and implications for Earth's earliest life. *Science* **296**, 1448–1452.

Fedo C. M. and Whitehouse M. J. (2002b) Origin and significance of Archean quartzose rocks at Akilia, Greenland. *Science* **298**, 917a.

Fletcher I. R., Kilburn M. R. and Rasmussen B. (2008) NanoSIMS μm-scale in situ measurement of $^{13}C/^{12}C$ in early Precambrian organic matter, with permil precision. *Int. J. Mass Spectrosc.* doi:10.1016/j.ijms.2008.08.010.

French B. M. (1973) Mineral assemblages in diagenetic and low-grade metamorphic iron-formation. *Econ. Geol.* **68**, 1063–1074.

French B. M. (1968) Progressive contact metamorphism of the Biwabik iron-formation, Mesabi Range, Minnesota. *Minn. Geol. Surv. Bull.* **45**, 1–47.

French B. M. (1964) Graphitization of organic material in a progressively metamorphosed Precambrian iron formation. *Science* **146**, 917–918.

Friend C. R. L., Nutman A. P. and Bennett V. C. (2002) Technical comment on origin and significance of Archean Quartzose Rocks at Akilia, Greenland. *Science* **298**, 917a.

Hayes J. M., Kaplan K. W. and Wedeking K. W. (1983) Precambrian organic geochemistry, preservation of the record. In *The Earth's Earliest Biosphere: Its Origin and Evolution* (ed. J. W. Schopf). Princeton University Press, NJ, pp. 93–134.

Horita J. (2005) Some perspectives on isotope biosignatures for early life. *Chem. Geol.* **218**, 171–186.

James H. L. (1955) Zones of regional metamorphism in the Precambrian of northern Michigan. *Bull. Geol. Soc. Am.* **66**, 1455–1488.

Jaszczak J., Dimovski S., Hackney S. A., Robinson G. W., Bosio P. and Gogotsi Y. (2007) Micro- and nanoscale graphite cones and tubes from Hackman Valley, Kola Peninsula, Russia. *Can. Mineral.* **45**, 379–389.

Kaufman A. J. (1996) Geochemical and mineralogic effects of contact metamorphism on banded iron-formation: an example from the Transvaal Basin, South Africa. *Precambrian Res.* **79**, 171–194.

Klein C. (2005) Some Precambrian banded iron-formations (BIFs) from around the world: their age, geologic setting, mineralogy, metamorphism, geochemistry, and origin. *Am. Mineral.* **90**, 1473–1499.

Klein C. (1978) Regional metamorphism of Proterozoic iron-formation, Labrador Trough, Canada. *Am. Mineral.* **63**, 912–998.

Klein C. (1973) Changes in mineral assemblages with metamorphism of some banded Precambrian iron formation. *Econ. Geol.* **68**, 1075–1088.

Konhauser K. O., Hamade T., Morris R. C., Ferris F. G., Southam G., Raiswell R. and Canfield D. (2002) Could bacteria have formed the Precambrian banded iron formations? *Geology* **30**, 1079–1082.

Konhauser K. O., Newman D. K. and Kappler A. (2005) The potential significance of microbial Fe(III)-reduction during Precambrian banded iron formations. *Geobiology* **3**, 67–177.

Konhauser K. O., Lalonde S. V., Amskold L. and Holland H. R. (2007) Was there really an Archean phosphate crisis. *Science* **315**, 1234.

Lattanzi P., Rye D. M. and Rice J. M. (1980) Behavior of ^{13}C and ^{18}O in carbonates during contact metamorphism at Marysville, Montana: implications for isotope systematics in impure dolomitic limestones. *Am. J. Sci.* **280**, 890–906.

Lepland A., Van Zuilen M. A., Arrhenius G., Whitehouse M. J. and Fedo C. M. (2005) Questioning the evidence for Earth's earliest life: Akilia revisited. *Geology* **33**, 77–79.

Lepland A., Arrhenius G. and Cornell D. (2002) Apatite in early Archean Isua supracrustal rocks, southern West Greenland: its origin, association with graphite and potential as a biomarker. *Precambrain Res.* **118**, 221–241.

Manning C. E., Mojzsis S. J. and Harrison T. M. (2006) Geology and age of supracrustal rocks, Akilia, Greenland. *Am. J. Sci.* **306**, 303–366.

McCollom T. M. and Seewald J. S. (2006) Carbon isotope composition of organic compounds produced by abiotic synthesis under hydrothermal conditions. *Earth Planet. Sci. Lett.* **243**, 74–84.

McGregor V. R. and Mason B. (1977) Petrogenesis and geochemistry of metabasaltic and metasedimentary enclaves in the Amîtsoq gneisses, West Greenland. *Am. Mineral.* **62**, 887–904.

McKeegan K. D., Kudryavtsev A. B. and Schopf J. W. (2007) Raman and ion microscopic imagery of graphitic inclusions in apatite from older than 3830 Ma Akilia Supracrustal rocks, west Greenland. *Geology* **35**, 591–594.

Mojzsis S. J., Coath C. D., Greenwood J. P., McKeegan K. D. and Harrison T. M. (2003) Confirmation of mass-independent isotope effects in Archean (2.5–3.8 Ga) sedimentary sulfides as determined by ion microprobe analysis. *Geochim. Cosmochim. Acta* **67**, 1635–1658.

Mojzsis S. J. and Harrison T. M. (2002a) Establishment of a 3.83-Ga magmatic age for the Akilia tonalite (southern West Greenland). *Earth Planet. Sci. Lett.* **202**, 563–576.

Mojzsis S. J. and Harrison T. M. (2002b) Origin and significance of Archean quartzose rocks at Akilia, Greenland. *Science* **298**, 917a.

Mojzsis S. J., Arrhenius G., McKeegan K. D., Harrison T. M., Nutman A. P. and Friend C. R. L. (1996) Evidence for life on Earth before 3,800 million years ago. *Nature* **384**, 55–59.

Myers J. S. and Crowley J. L. (2000) Vestiges of life in the oldest Greenland rocks? A view of early Archean geology in he Godthabsfjord region, and reappraisal of field evidence for >3850 Ma life on Akilia. *Precambrian Res.* **103**, 101–124.

Naraoka H., Ohtake M., Maruyama S. and Ohmoto H. (1996) Non-biogenic graphite in 3.8-Ga metamorphic rocks from the Isua district, Greenland. *Chem. Geol.* **133**, 251–260.

Nutman A. P. and Friend C. R. L. (2006) Petrography and geochemistry of apatites in banded iron formation, Akilia, W. Greenland: consequences for oldest life evidence. *Precambrian Res.* **147**, 100–106.

Nutman A. P., Mojzsis S. J. and Friend C. R. L. (1997) Recognition of $\geqslant$3850 Ma water-lain sediments in West Greenland and their significance for the early Archaean Earth. *Geochim. Cosmochim. Acta* **61**, 2475–2484.

Oehler D. Z., Robert F., Mostefaoui S., Meibom A., Selo M. and McKay D. S. (2006) Chemical mapping of Proterozoic organic matter at sub-micron spatial resolution. *Astrobiology* **6**, 838–850.

Oehler D. Z., Robert F., Walter M. R., Sugitani K., Allwood A., Meibom A., Mostefaoui S., Selo M., Thomen A. and Gibson E. K. (2009) NanoSIMS: insights to biogenecity and syngenecity of Archean carbonaceous structures. *Precambrian Res.* **173**, 70–78.

Ohmoto H. and Rye R. O. (1979) Isotopes of sulfur and carbon. In *Geochemistry of Hydrothermal Ore Deposits* (ed. H. L. Barnes), second ed. Wiley, New York, NY, pp. 509–567.

Papineau D., DeGregorio B. T., Cody G. D., Fries M. D., Mojzsis S. J., Steele A., Stroud R. M. and Fogel M. L. (2010) Ancient graphite in the Eoarchean quartz–pyroxene rock from Akilia Island in southern West Greenland I: Petrographic and spectroscopic characterization. *Geochim. Cosmochim. Acta* **74**, 5862–5883.

Papineau D. (2010) Global biogeochemical changes at both ends of the Proterozoic: insights from phosphorites. *Astrobiology* **10**, 165–181.

Pasteris J. D. (1989) In situ analysis in geological thin-sections by laser Raman microprobe spectroscopy: a cautionary note. *Appl. Spectrosc.* **43**, 567–570.

Rumble D., Duke E. F. and Hoering T. L. (1986) Hydrothermal graphite in New Hampshire: evidence of carbon mobility during regional metamorphism. *Geology* **14**, 452–455.

Rumble D. and Hoering T. L. (1986) Carbon isotope geochemistry of graphite vein deposits from New Hampshire, USA. *Geochim. Cosmochim. Acta* **50**, 1239–1247.

Rushdi A. I. and Simoneit B. R. T. (2005) Abiotic synthesis of organic compounds from carbon disulfide under hydrothermal conditions. *Astrobiology* **5**, 749–769.

Rushdi A. I. and Simoneit B. R. T. (2004) Condensation reactions and formation of amides, esters, and nitriles under hydrothermal conditions. *Astrobiology* **4**, 211–224.

Sano Y., Terada K., Takahashi Y., Nutman A. P., Mojzsis S. J., Harrison T. M., Arrhenius G., McKeegan K. D. and Grove M. (1999) Origin of life from apatite dating? *Nature* **400**, 127–128.

Schneider D. A., Bickford M. E., Cannon W. F., Schulz K. J. and Hamilton M. A. (2002) Age of volcanic rocks and syndepositional iron formations, Marquette Range Supergroup: implications for the tectonic setting of Paleoproterozoic iron formations of the Lake Superior region. *Can. J. Earth Sci.* **39**, 999–1012.

Schulz K. J. and Cannon W. F. (2007) The Penokean orogeny in the Lake Superior region. *Precambrian Res.* **157**, 4–25.

Schreyer W., Stepto D., Abraham K. and Muller W. F. (1978) Clinoeulite (magnesian-clinoferrosilite) in a eulysite of a metamorphosed iron formation in Vredofort Structure, South Africa. *Contrib. Mineral. Petrol.* **65**, 351–361.

Sims P. K., Van Schmus W. R., Schulz K. J. and Peterman Z. E. (1989) Tectono-stratigraphic evolution of the Early Proterozoic Wisconsin magmatic terranes of the Penokean Orogen. *Can. J. Earth Sci.* **26**, 2145–2158.

Steele A., Fries M. D., Amundsen H. E. F., Mysen B. O., Fogel M. L., Schweizer M. and Boctor N. Z. (2007) Comprehensive imaging and Raman spectroscopy of carbonate globules from Martian meteorite ALH 84001 and a terrestrial analogue from Svalbard. *Meteor. Planet. Sci.* **42**, 1549–1566.

Strauss H., DesMarais D. J., Hayes J. M. and Summons R. E. (1992) Concentrations of organic carbon and maturities and elemental compositions of kerogens. In *The Proterozoic Biosphere: A Multidisciplinary Study* (eds. J. W. Schopf and C. Klein). Cambridge University Press, Cambridge, pp. 5–99.

Tan P. H., Dimovski S. and Gogotsi Y. (2001) Raman scattering of non-planar graphite: arched edges, polyhedral crystals, whiskers, and cones. *Philos. Trans. R. Soc. Lond. A* **362**, 2289–2310.

Ueno Y., Yurimoto H., Yoshioka H., Komiya T. and Maruyama S. (2002) Ion microprobe analysis of graphite from ca. 3.8 Ga metasediments, Isua supracrustal belt, West Greenland: relationship between metamorphism and carbon isotopic composition. *Geochim. Cosmochim. Acta* **66**, 1257–1268.

Valley J. W. (1986) Stable isotope geochemistry of metamorphic rocks. In *Stable Isotopes in High Temperature Geological Processes*, vol. 16 (eds. J. W. Valley, H. P. Taylor and J. R. O'Neil). Mineralogical Society of America, Washington, DC, pp. 445–489.

Van Cappellen P. and Berner R. A. (1988) A mathematical model for the early diagenesis of phosphorus and fluorine in marine sediments: apatite precipitation. *Am. J. Sci.* **288**, 289–333.

van Zuilen M. A., Lepland A. and Arrhenius G. (2002) Reassessing the evidence for the earliest traces of life. *Nature* **418**, 627–630.

van Zuilen M. A., Mathew K., Wopenka B., Lepland A., Marti K. and Arrhenius G. (2005) Nitrogen and argon isotopic signatures in graphite from the 3.8-Ga-old Isua Supracrustal Belt. *Geochim. Cosmochim. Acta* **69**, 1241–1252.

Wacey D., Kilburn M. R., McLoughlin N., Parnell J., Stoakes C. A., Grovenor C. R. M. and Brasier M. D. (2008) Use of nanoSIMS in the search for early life on Earth: ambient inclusion trails in a ca. 3400 Ma sandstone. *J. Geol. Soc. Lond.* **165**, 43–53.

Whitehouse M. J., Myers J. S. and Fedo C. M. (2009) The Akilia Controversy: field, structural and geochronological evidence questions interpretations of >3.8 Ga life in SW Greenland. *J. Geol. Soc. Lond.* **166**, 335–348.

Whitehouse M. J. and Kamber B. S. (2005) Assigning dates to thin gneissic veins in high-grade metamorphic terranes: a cautionary tale from Akilia, southwest Greenland. *J. Petrol.* **46**, 291–318.

Whitehouse M. J. and Fedo C. M. (2003) Deformation features and critical field relationships of early Archean rocks, Akilia, southwest Greenland. *Precambrian Res.* **126**, 259–271.

Wopenka B. and Pasteris J. D. (1993) Structural characterization of kerogens to granulite facies graphite: applicability of Raman microprobe spectroscopy. *Am. Mineral.* **78**, 533–557.

Associate editor: Juske Horita